Experimental Investigation of Nonlinear Mode Shape in Microscale Beams

An Undergraduate Honor Thesis

Presented in Partial Fulfillment of the Requirements for Graduation with Distinction

Mechanical Engineering at The Ohio State University

By

Min Ma

The Ohio State University

Spring, 2017

Committee: Dr. Hanna Cho; Dr. Jason Dreyer

Abstract

Micro-electro-mechanical-systems (MEMS) have drawn a great interest over last serval decades due to its wide applications including accelerometers and pressure sensors, micro-mirrors, radiofrequency (RF) switches, microphones, and inertia sensors. The moving mechanical element integrated in MEMS devices is typically operating in its resonant mode. Due to its small size and low damping, the micro-beams often exhibit the nonlinear resonance, which is being widely investigated to overcome the limitations of linear mode in term of its levels of sensitivity and reliability. This work covers an experimental study of the dynamic responses of micro-beams, including the nonlinear mode shape and resonances by improving the experimental tool and accuracy. The characterization is performed on a silicon-polymer micro-beam that is excited near its fundamental mode frequency by a piezoelectric shaker. The nonlinearity of this micro-beam originates geometrically from the elongation of the polymer part during large flexural oscillations of the silicon part. Its amplitude of oscillation is detected by Laser Doppler Vibrometer (LDV) while the excitation frequency is varied. To study the nonlinear mode shape, the points of measurement are scanned along the longitudinal direction of the micro-beam located on a 2-axis piezoelectric stage. A custom LabVIEW program which can precisely control the movable stage and collect the vibration amplitude data at different locations was developed. The experimental measurement provides the most realistic mode shape of the micro-beam and gives a better understanding of the vibration behavior of MEMS resonators.

Acknowledgments

First and foremost, I would like to thank my research advisor, Professor Hanna Cho. Without her guidance and dedicated involvement in every step throughout the process, this paper would have never been accomplished. I would like to thank her very much for her support and understanding over the past year on this project.

I greatly appreciate Mr. Keivan Asadi's help. He has being so generous with his time in processing partial experiment data and explaining to me. I also would to like to thank for Dr. Hatem Brahmi for his time revising my thesis and fundamental explanation of this research.

Vita

June, 1991 ---------- Changzhi, China

2010 to 2012 ---------- Xiamen University, China

2013 to 2014 ---------- Arizona State University, U.S.A

2014 to 2017 ---------- Ohio State University, U.S.A

Fields of Study

Major Field: Mechanical Engineering

Table of Contents

List of Figures

List of Tables

Chapter 1: Introduction

1.1 Motivation

Several decades have passed by since the discovery and development of micro-electro-mechanical-systems (MEMS). This technology has reached a level of maturity that delivers commodity products for our everyday life, such as integrated multi-sensor modules (9 degrees-of-freedom inertial, gas, pressure, temperature, and flow), actuators (inkjet nozzles, digital mirror displays), communication components (RF filters, oscillators, duplexers), and other transducers (power harvesters). Nowadays, hundreds of foundries around the world offer numerous fabrication services that can translate the imagination of a MEMS designer of a device into reality. Even with the development of fabrication processes and commercialization, MEMS are still one of the hottest evolving areas in science and engineering. Scientists from across various disciplines investigate, brainstorm, and collaborate to invent smarter devices, develop new technologies, and innovate unique solutions. The forecasts for the MEMS market shows a compound annual growth rate of 5–24% for the period 2013–2019 [1]. The increasing impact that MEMS have on markets is caused by their typically small size, which makes them minimally invasive into larger systems.

The easiest way to introduce MEMS is referring to the acronym MEMS itself. MEMS stands for micro-electro-mechanical-systems. Hence, they are devices in the “micro” scale, in which one or more of their dimensions are in the micrometer range. The “electro” part indicates that they use electric signals and power. “Mechanical” means these devices rely on some sort of mechanical motion, action, or mechanism. The word “system” refers to the fact that they function as integrated systems and not

as individual components. Thereby, MEMS are attributed to the integration of mechanical elements, sensors, actuators, and electronics on a common silicon substrate through micro-fabrication technology.

MEMS technology covers different fields including sensors, actuators, RF-MEMS, Optical-MEMS, Microfluidic-MEMS, and Bio-MEMS [2]. So far the sensor industry is the most-developed and productive sector for MEMS and shows top-notch technology with high efficiency and long life performance. Examples of MEMS sensor areas include pressure sensors, accelerometers, gas and mass sensors, temperature sensors, force sensors, and humidity sensors. Historically speaking, the early generation of MEMS researchers has relied on journals and conferences of sensors and actuators to disseminate their research on miniature devices before the introduction of specialized MEMS conferences and journals in the early 1990s.

The fascination in the MEMS technology comes from their distinguished characteristics. MEMS are characterized by low cost which is a direct consequence of the batch fabrication. This means that each fabrication batch can produce thousands of MEMS devices all at once. They are lightweight and small which is desirable for compactness and convenience reasons. The fabrication of MEMS devices usually starts with single crystal silicon wafers which come in many standard sizes. Silicon is the ideal material due to its excellent thermal and mechanical properties [2] (stable mechanism, high melting point, high toughness, and smallest thermal expansion coefficient). In addition, their small size allows the implementation of MEMS in tight locations where large devices do not fit, such as engines in cars [3] and inside the human body [4]. Moreover, they consume very low power which not only reduces the operational cost but also enables the development of long-life and self-powered devices that can

harvest a small amount of energy they need from the environment during their operation. Furthermore, MEMS devices have enabled many superior performances, smart functionalities, and complicated tasks that cannot be achieved in other technologies. For proof of their uniqueness one can cite examples of ultra-sensitive mass detectors [5], high isolation and low-insertion-loss RF switches [6], lab-on-a-chip bio-sensors [6], tiny directional microphones for hearing aids [6], high-temperature pressure sensors for automobile engines [6], and precise controlled liquid droplets for ink-jet printers [6].

According to the International Technology Roadmap for Semiconductors [7], current MEMS technologies will not be able to meet the next decade's systems requirement in terms of performance, functionalities, power consumption, cost, and size. The challenge of MEMS can be classified into three broad categories: nonlinearities, interdisciplinary, and microscale phenomena.

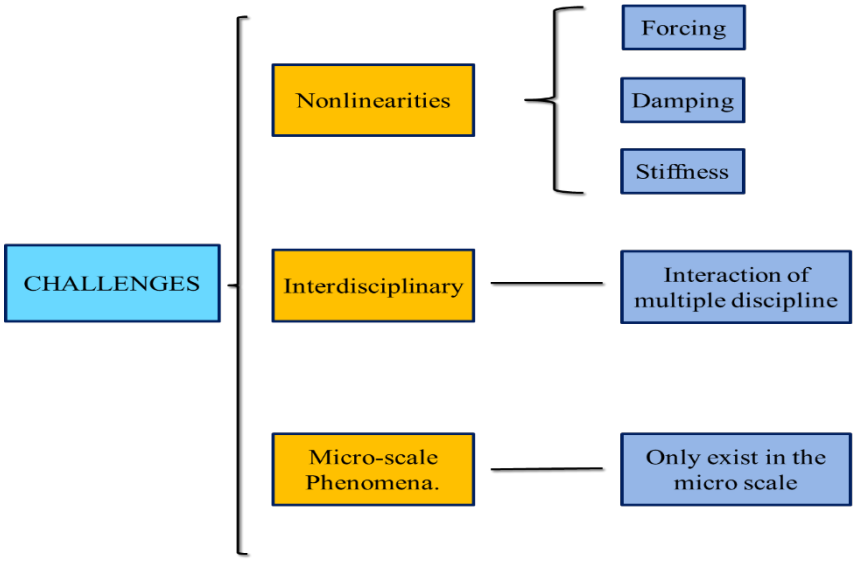

Figure 1: Challenge of MEMS

Nonlinearities in MEMS resonators have different origins [8] [9]. One of main sources of nonlinear effect is the geometric effect [8]. When microstructures are actuated, they can easily undergo relatively large motions (compared to its thickness) and geometric nonlinearities of the structures are amplified. In the macro-scale world, the vibration of objects, such as bridges and buildings, is typically small

compared to their dimensions due to their large damping. Hence, it is commonly acceptable to apply linear theories to study their deformation and motion. In a microscale structure, however, the relative motion becomes comparable to its thickness and size due to small damping of the structure. The mid-plane stretching leads to the increase of its stiffness and change of dynamical behavior. In addition to the nonlinear stiffness, forcing and damping can also produce nonlinearities through actuation and detection mechanisms. Many complex damping mechanisms can happen unlike in a macroscale system. For example, the squeeze-film damping, which is inherently nonlinear (inversely proportional to the cubed distance between the close surfaces), often happens in microscale systems.

The second challenge of MEMS originates from the interdisciplinary nature of MEMS while various energy domains and physical forces, such as mechanical, fluidic, thermal, and electrical forces co-exist in the system. Hence, analyzing the behavior of a typical MEMS device requires the knowledge in more than one discipline and the ability to deal with the interaction and interface issues over various fields.

The third category of challenge of MEMS is micro-scale phenomena which have less effect on the macro-scale structure but has significant impact on micro-scale structures. When the dimensions of an object are reduced by x, the volume and hence the mass is reduced by a factor of x^3. On the other hand, the mechanical force is reduced by x while the inertial force it can generate is reduced by x^3. A major benefit of this phenomenon is that MEMS can withstand tremendous accelerations (more than 100,000 g force acceleration) without breaking. Such drastic changes of physical quantities in MEMS compared to macroscale systems require a total paradigm shift in the mindset for a designer.

Many researchers and engineers focus on the mechanical behavior of MEMS devices and their statics and dynamics behavior to improve the performance of MEMS. In this work, we focus on understanding nonlinear behavior of MEMS devices induced by the geometric originations. The linear dynamics of microstructure, such as micro beam or microcantilever, are successfully predicted by Euler-Bernoulli theory [9]. Even though the nonlinear resonance has been widely investigated in both theoretical and experimental ways, the nonlinear mode shape of various mirco-resonators has not been studied rigorously.

1.2 Objective

The first purpose of this research is to characterize the dynamic behavior of two type micro-beams by experimentally capturing their nonlinear mode shape. To do so**,** measurement of the vibration amplitude was performed at multiple scan points using Laser Dropper Vibrometer. Then the collected data was processed and analyzed in MATLAB to extract the vibration mode shape.

The second purpose of this research is to improve the current measurement setup. To achieve this goal, the capability of an existing experimental setup was enhanced by integrating an automated scan of different locations of the vibrating micro-beams**.** Using a piezoelectric linear stage, an accurate scan step as small as 4 nm was achieved. All the measurement equipment was controlled through one main LabVIEW program.

Chapter 2: Fundamental Background

2.1 Linear Vibration

2.1.1 Dynamics of single degree of freedom systems

Many MEMS devices are modeled as lumped or concentrated mass, spring, damper and driven force. The discussion will start with a single-degree-of-freedom (SDOF) system, shown in Figure 2. The first step in the vibration analysis is deriving the equation of motion for the system.

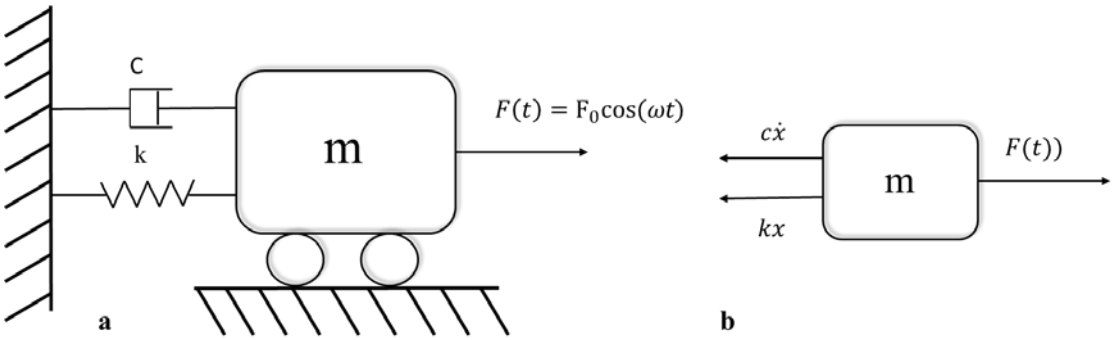

Figure 2: Spring-Mass-Damper System

Newtown's second law of motion is used:

$$\sum \vec{F} = m\ddot{x} \qquad \textit{Equation 2.1}$$

where $\sum \vec{F}$ represents the sum of forces acting on the mass *m* and $\ddot{x}$ is the acceleration of the mass. To apply equation (2.1) on the system, the mass is assumed to be displaced in the positive direction (to the right) by a distance *x*. Figure 2b represents the free-body-diagram of the system. The force relationship of the spring and damper is

$$\overrightarrow{F_s} = -kx \qquad \textit{Equation 2.2}$$

$$\overrightarrow{F_d} = -c\dot{x} \qquad \textit{Equation 2.3}$$

where *k* is the spring stiffness, *c* is the damping coefficient, and the negative sign indicates that the force is in the opposite direction of motion. The systems are driven by a harmonic force excitation given by

$$F(t) = F_o cos(\omega t) \qquad \textit{Equation 2.4}$$

where F_o is the harmonic force amplitude and ω is the excitation frequency. Appling Eqs. 2.2-2.4, we get the second order, linear ordinary differential equation governing the displacement of the SDOF system:

$$m\ddot{x} + c\dot{x} + kx = F_o co\, s(\omega t). \qquad \textit{Equation 2.5}$$

Dividing Equation 2.5 by *m* yields

$$\ddot{x} + 2\xi\omega_n\dot{x} + \omega_n^2 x = f_o cos(\omega t) \qquad \textit{Equation 2.6}$$

where $f_o = \frac{F_0}{m}$, and ξ is the damping ratio, a nondimensional quantity described by

$$\xi = \frac{c}{2m\omega_n} \qquad \textit{Equation 2.7}$$

where ω_n is called underdamped natural frequency in rad/sec, defined as:

$$\omega_n = \sqrt{k/m} \qquad \textit{Equation 2.8}$$

The steady state response of this system can be written as:

$$x(t) = A\, cos(\omega t) + Bsin(\omega t) \qquad \textit{Equation 2.9}$$

A more convenient way to express this solution is:

$$x(t) = Acos(\omega t - \theta) \qquad \textit{Equation 2.10}$$

where

$$A = \frac{f_0}{\sqrt{\left(\omega_n^2 - \omega^2\right)^2 + (2\xi\omega_n\omega)^2}} \qquad \textit{Equation 2.11}$$

$$\theta = tan^{-1}\left(\frac{2\xi\omega_n\omega}{\omega_n^2 - \omega^2}\right) \qquad \textit{Equation 2.12}$$

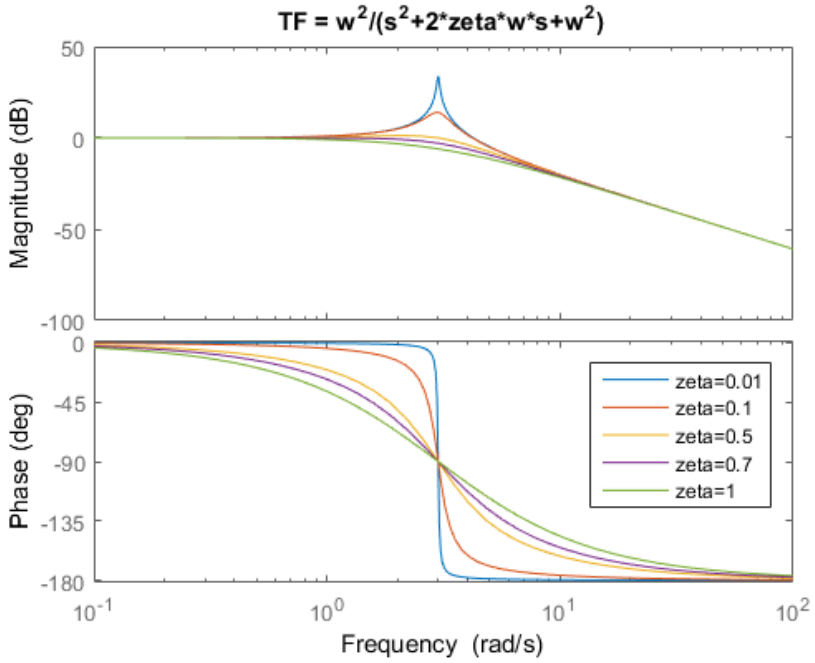

Figure 3: Bode plot for different zeta values

Figure 3 shows the amplitude *A* and phase angle θ of the spring-mass-damper system when the input frequency is varied. The frequency response of a small ξ (smaller than 0.707) has a peak near $\omega = \omega_n$, called resonance phenomenon. When the excitation frequency is equal or near to the natural frequency, the system with low damping oscillates at a large amplitude. A system with ξ larger than 0.707 does not have any peak, i.e., no resonance occurs. Most MEMS resonators exhibit this resonance behavior owing to the lower values of damping ratio. In MEMS, quality factor Q is more commonly used to characterize the system's damping, defined as:

$$Q = \frac{1}{2\xi} \qquad \textit{Equation 2.13}$$

Q factor describes how an under-damped oscillator or resonator is and characterizes a resonator's bandwidth relative to its center frequency. Higher Q indicates a lower rate of energy loss relative to the stored energy of the resonator and a higher oscillation amplitude, as shown in Fig. 3.

2.1.2 Dynamics of a continuous system

Most realistic systems are continuous and have an infinite number of degrees of freedom. When the dynamics of a continuous beam structure is theoretically analyzed, it is often approximated as multi-degree of freedom (MDOF) systems by including initial few modes to seek simplicity of analysis. It is generally sufficient to consider only the first three or four modes for a simple beam structure, since the higher modes are quickly decayed by damping. For a system having *n* degrees of freedom, there exist *n* number of mode frequencies and each associated mode shapes. Figures 4-5 show the first several mode shapes and frequencies of a beam with fixed-free boundary conditions and with fixed-fixed boundary conditions, respectively. A beam can be thought of as a series of spring-mass-damper models joined to form a continuous system. When the beam vibrates, these modes are superimposed one another to give the overall response of the system.

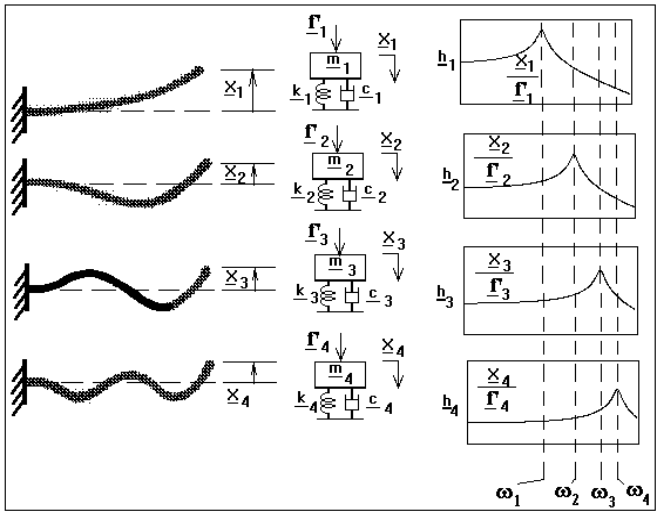

Figure 4: Linear mode shapes of cantilever beam and corresponding frequency response (http://signalysis.com/)

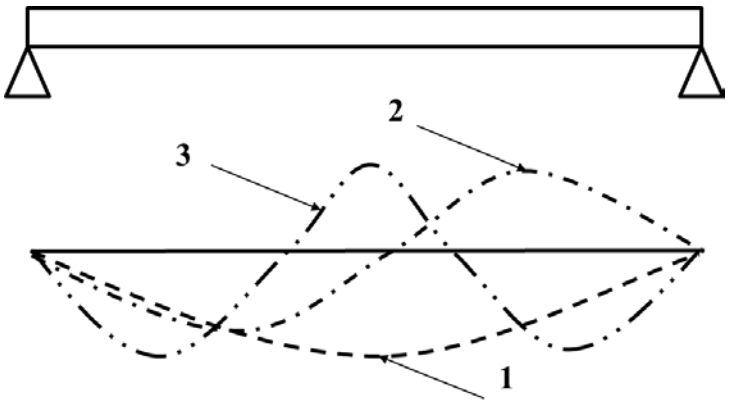

Figure 5: Linear mode shape (1st, 2nd and 3rd modes) of a fixed-fixed beam

To derive the mode shape and mode frequency analytically, the beam structure should be modeled more accurately as a continuous or distributed-parameter system of distributed mass, stiffness, damping, and forcing. Its dynamical behavior is then governed by a partial differential equation that vary in space and time as opposed to the ordinary differential equation in time like in the case of lumped-parameter systems.

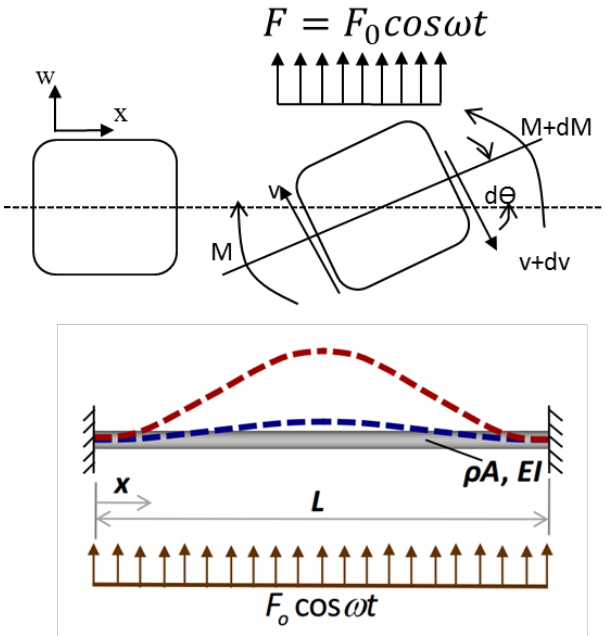

Figure 6: Free body diagram of a section of beam under transverse vibration

Figure 6 shows a beam in the bending condition. The beam undergoes transverse vibration under the distributed loading. The free body diagram is shown in the top of Fig. 6. The method used to analyze the bending moment is called Euler–Bernoulli beam theory [9]. The $F(x,t)$ is the external force with respect to time and location. M is the bending moment, V is the shear force, and N is the tensile axial force. The derived equation of bending motion for the forced transverse beam is called Euler-Bernoulli beam equation, as shown in equation below:

$$\rho A \frac{\partial^2 w(x,t)}{\partial t^2} + EI \frac{\partial^4 w(x,t)}{\partial x^4} = F(x,t) \qquad \textit{Equation 2.14}$$

when ρ is the density, A is cross section, E is the young's module, and I is the area moment of inertia.

By using the separation of variables, $w(x,t)$ can be separated as the multiplication of the time dependent variable and the displacement dependent variable,

$$w(x,t) = W(x)T(t) \qquad \textit{Equation 2.15}$$

Substituting equation 2.15 into equation 2.14, the governing equation is separated into two ordinary differential equations:

$$\ddot{T} + \omega^2 T = 0 \qquad \textit{Equation 2.16}$$

$$W'''' - \frac{m\omega^2}{EI} W = 0 \qquad \textit{Equation 2.17}$$

where the general solution of W(x) and T (t) are:

$$T(t) = A\cos(\omega t) \qquad \textit{Equation 2.18}$$

$$\mathrm{W(x)} = \mathrm{c_1}\cos(\beta \mathrm{x}) + \mathrm{c_2}\sin(\beta \mathrm{x}) + \mathrm{c_3}\cosh(\beta \mathrm{x}) + \mathrm{c_4}\sinh(\beta \mathrm{x}) \qquad \textit{Equation 2.19}$$

Equation 2.19 is the mode shape function. c_1, c_2, c_3, c_4 and β are constant which can be found by applying the boundary conditions.

For a cantilever beam with free-fixed boundary conditions, shown in Fig. 7, the following boundary conditions will be involved to express the mode shape function of cantilever beam.

$$W|_{x=0} = 0,\ \frac{dW}{dx}|_{x=0} = 0,\ \frac{d^2W}{dx^2}|_{x=L} = 0,\ \frac{d^3W}{dx^3}|_{x=L} = 0 \qquad \textit{Equation 2.21}$$

Substituting equation 2.21 into equation 2.19 gives

$$\mathrm{W(x)} = \cosh(\beta \mathrm{x}) - \cos(\beta \mathrm{x}) + \left(\frac{\cosh(\beta L)+\cos(\beta L)}{\sinh(\beta L)+\sin(\beta L)}\right)(\sin(\beta \mathrm{x}) - \sinh(\beta \mathrm{x})) \qquad \textit{Equation 2.22}$$

where βL is 1.8751, 4.6940, 7,8547 for the first three modes.

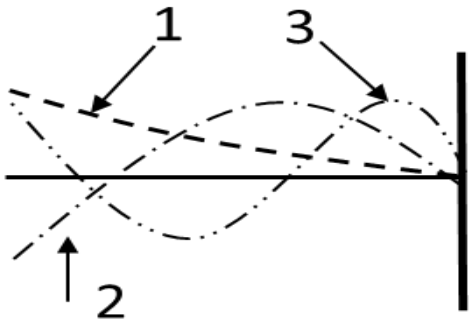

Figure 7: Mode shape of Cantilever beam

2.2 Nonlinear Vibration

To understand the dynamics of a nonlinear system, here a spring-mass-damper system with nonlinear spring stiffness is considered.

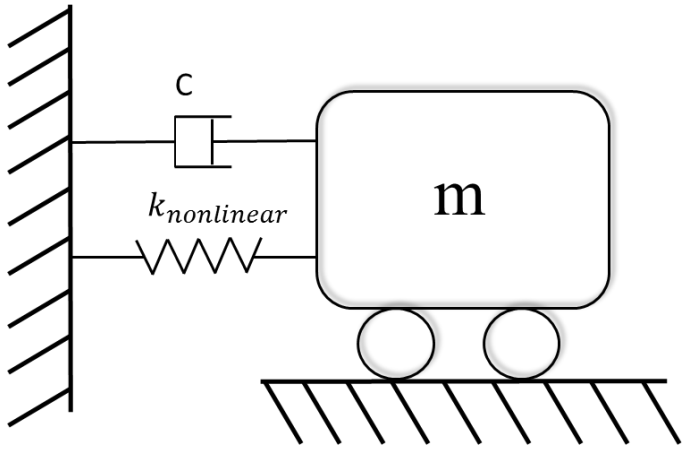

Figure 8: SDOF spring-mass- damper system with nonlinear stiffness

The spring force in system is nonlinear, which is expressed by:

$$F = k_1 x + k_2 x^2 + k_3 x^3 \qquad \textit{Equation 2.23}$$

Therefore, the equation of motion of this system is defined as:

$$m\ddot{x} + c\dot{x} + k_1 x + k_2 x^2 + k_3 x^3 = 0 \qquad \textit{Equation 2.24}$$

The real mode of micro-beams involves the nonlinear behavior, and it is induced when a beam undergoes moderately large deflection compared to its thickness. In this case, the beam tends to stretch and experience a large deformation. This induces the tensile axial stress, thereby changing the stiffness of the beam in a nonlinear way that resembles a cubic effect. Here, we assume a planar motion, linear stress–strain law, and initially straight beam. For simplicity, the beam properties E, I, A, and ρ are assumed constant. The Euler-Bernoulli beam equation, equation 2.14 needs to be changed as:

$$\rho A \frac{\partial^2 w}{\partial t^2} + EI \frac{\partial^4 w}{\partial x^4} = T \frac{\partial^2 w}{\partial x^2} + F \qquad \textit{Equation 2.21}$$

where T is the tension in the beam. The tension is:

$$\frac{\Delta L}{L} = \frac{\int_0^L dw \sqrt{1+\left(\frac{\partial w}{\partial x}\right)^2} - L}{L} \qquad \textit{Equation 2.22}$$

$$T = EA\frac{\Delta L}{L} = \frac{EA}{2L}\int_0^L dw \left(\frac{\partial w}{\partial x}\right)^2 \qquad \textit{Equation 2.23}$$

Substituting equation 2.22 and equation 2.23 into equation 2.21 will give the final expression of nonlinear equation of motion:

$$\rho A \frac{\partial^2 y}{\partial t^2} + c\frac{\partial y}{\partial t} + EI\frac{\partial^4 y}{\partial t^4} - \frac{EA}{2L}\int_0^L dy \left(\frac{\partial y}{\partial x}\right)^2 = F\cos\omega t \qquad \textit{Equation 2.24}$$

Figure 9 shows how the linear resonance transits to the nonlinear resonance when the excitation force is increased. As the oscillation amplitude becomes larger than a critical value, the resonance curve bends toward higher frequencies due to the stiffness hardening effect.

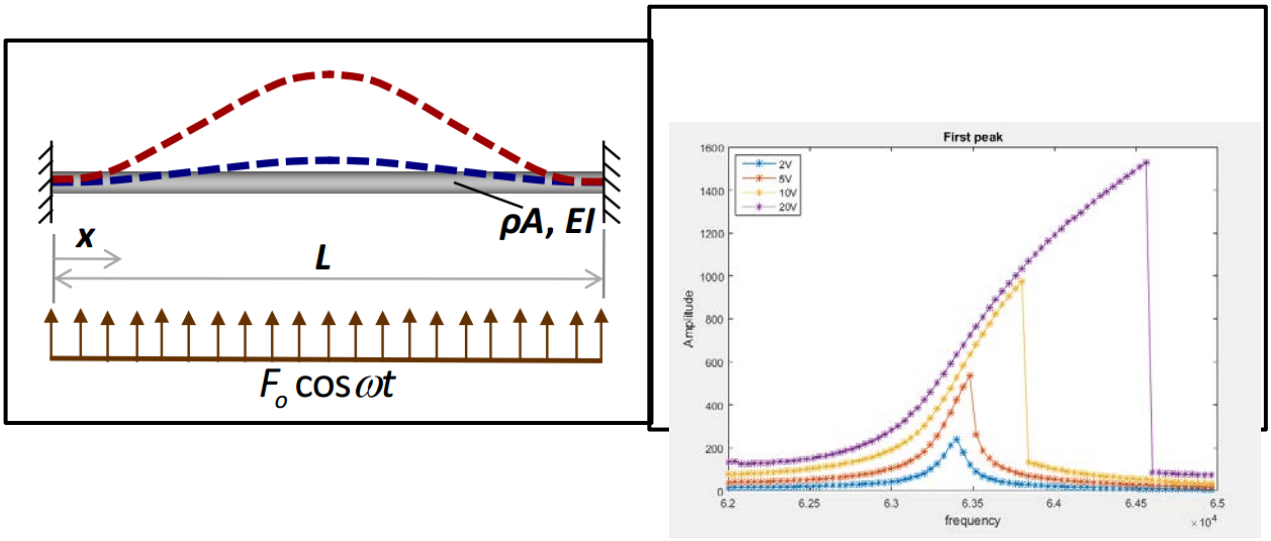

Figure 9: Linear and Nonlinear response

Chapter 3. Experiment Setup and Measurements

3.1 Experimental setup

In this section, we present the different equipment used to set up the experimental measurement of vibration amplitude for micro beam. An existing setup was built and used for the same purpose but it allows only single point measurement of vibration amplitude. The setup is mounted on top of an optical table to eliminate parasitic vibrations as it is shown in the figure 10a and figure 10b. The setup consists of one function generator (TEKTRONIX, type AFG3022C) used to apply voltage to the piezoelectric shaker and this is the actuation part. Laser Doppler Vibrometer (Polytech) and its controller are used to detect the beam deflection. Both the function generator and the LDV controller are connected to an oscilloscope as signal converter and reader. The sample used to be mounted on a metal substrate to the shaker, then in the new setup it will be mounted to a micro stage (described later).

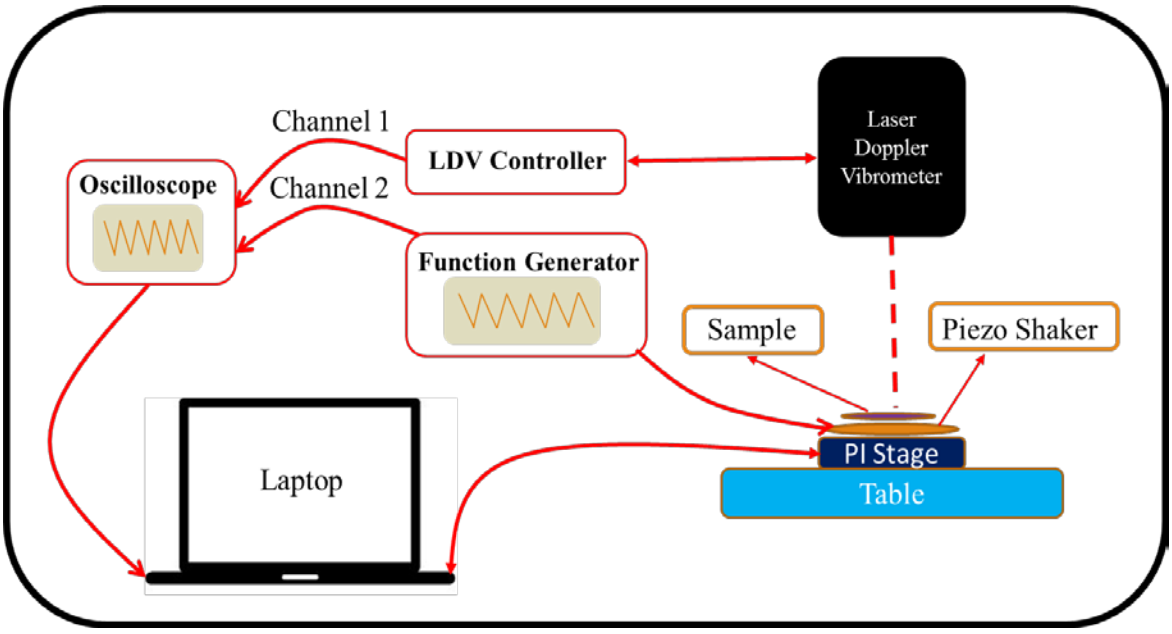

Figure 10:Sechmatic experimental setup

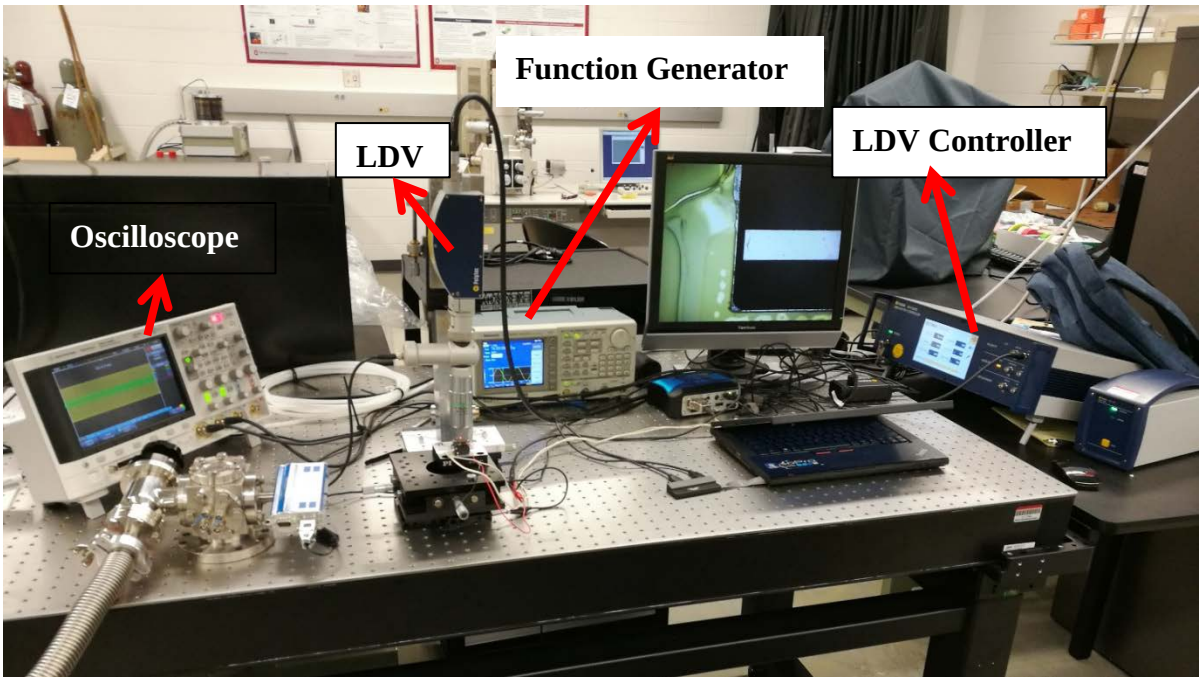

Figure 11: Experimental setup

The shaker could be biased with different DC voltages (maximum of 20V) and induces vibration in the microbeam structure. The static deflection of the beam is captured using the Laser Doppler Vibrometer (LDV). LDV is used to make non-contact vibration measurements of a surface. The laser beam from the LDV is directed to the surface of interest, and the vibration amplitude and frequency are extracted from the Doppler shift of the reflected laser beam frequency due to the motion of the surface. The actual LDV gives a frequency range up to 24 MHz, with velocity up to 10 m/s and displacement range from picometer to meter. The electric signal has been detected by the LDV is transferred to the oscilloscope.

In this case study, channel one of the oscilloscope is connected to function generator, channel two is connected to vibrometer controller. The measurement results give three quantities: first is the amplitude of vibration which is measured by vibrometer controller and transfer the electric signal to

oscilloscope, and two phase shift, one is given by function generator and another is measured by vibrometer controller. The difference between the two phases represent sample's phase shift of vibration. All the equipment are controlled using one LabVIEW program that allow to set the input parameters and read the output data.

The current measurement setup provides single point measurement of the vibration amplitude, however and to capture the mode shape experimentally we need to perform measurements in different locations on the beam. Thus it comes the idea of scanning the beam surface by moving the body of the beam under the laser point (fixed). For this purpose we used a piezoelectric stage, shown in figure 11.

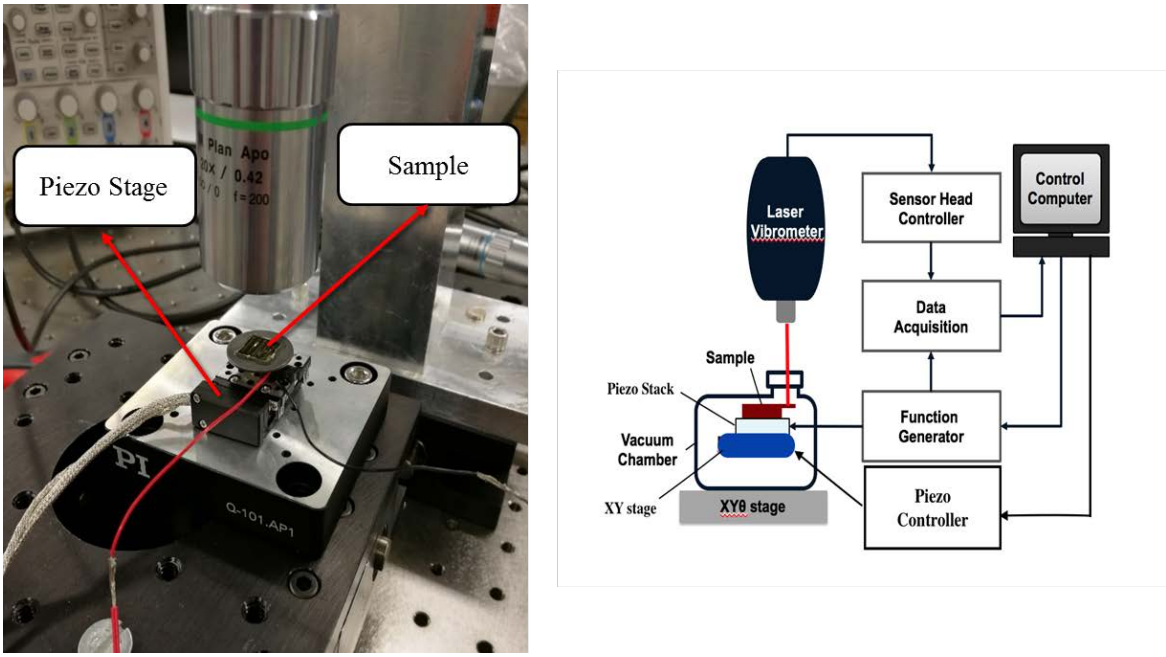

Figure 12: Piezoelectric stage

The piezoelectric stage is automatically moving under prescribed given voltage and provides precisely controllable movement in multiple locations in the beam surface. The piezoelectric effect is core principle to manipulate the stage. The piezoelectric effect is a reversible process: the direct piezoelectric effect corresponds to the internal generation of electrical charge from an applied

mechanical force, and the reverse piezoelectric effect consists of the internal generation of a mechanical displacement under applied electrical field. The piezoelectric stage is fabricated by Physik Instrumente (PI), type Q-522. It is 22 mm wide and 10 mm high and provides displacement within a maximum travel range of 6.5mm and with a resolution (smallest displacement) down to 4nm. The velocity of stage is up to 10 mm/ s. and it can hold 1 N force.

LabVIEW [10] software is used to control the stage movement as well as the input/output signals thus the communication between the equipment and the computer. The software consists of a collection of virtual instrument (VI) drivers. All functionalities involves one or more VIs with the appropriate parameters and variables settings.

The main program is built subprograms that provide measurement values of the maximum amplitude and phase value of the vibrating beam at each scan point, and in the same time it allows to control the movement of the piezoelectric stage hence the scan along the beam. Figure 12 show the logic statement of piezoelectric stage operation.

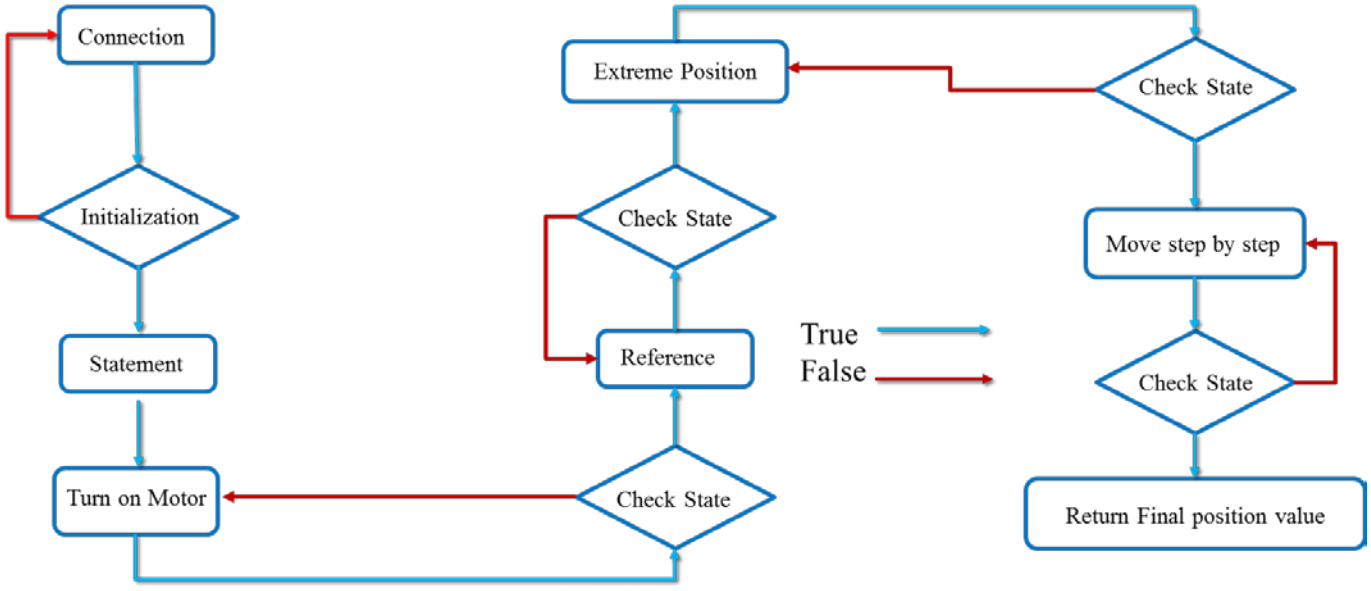

Figure 13: Logic Statement of moving piezoelectric stage

3.2 Measurement Procedure

The measurement will be conducted on two different structures: the first one is a silicon micro cantilever (clamped-free beam) (Fig.13) and the second one is a clamped-clamped micro beam structure. The double clamped beam consists of two parts: silicon part and small polymer attachment with the dimensions mentioned previously and shown in the Scanning Electron Microscope (SEM) image (Fig.14). The SEM produces images of a sample by scanning it with a focused beam of electrons.

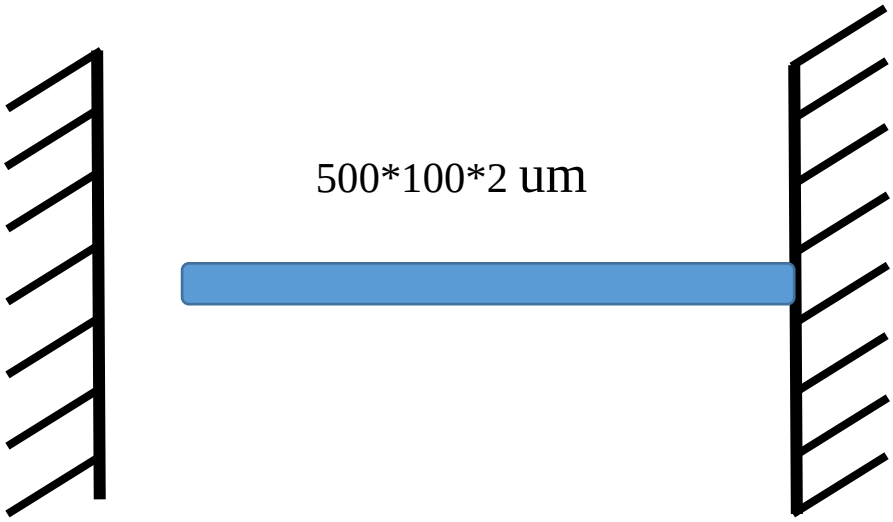

Figure 14: Schematic image of the silicon beam microstructure

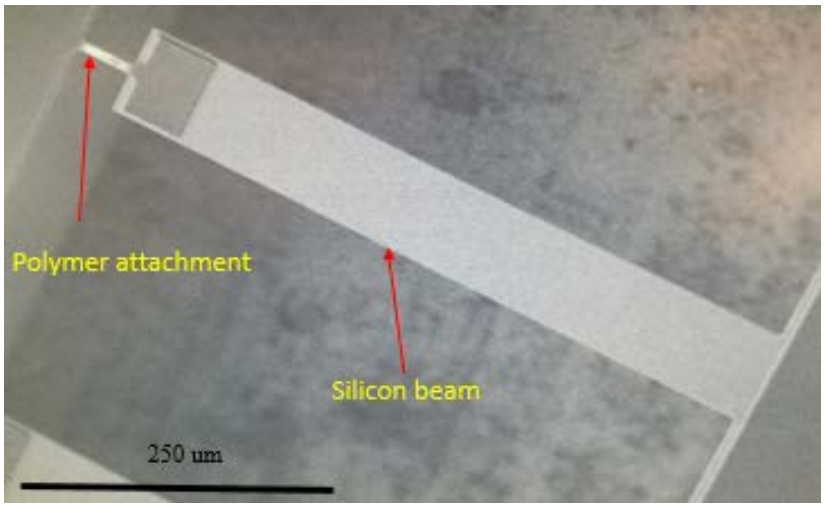

Figure 15: SEM image of the silicon beam/polymer microstructure

First step of the measurement is to determine the thermal frequency of micro-beam. The thermal frequency is natural frequency caused by thermal effect. It is broadband excitation due to the thermal loading inherent to micro-scaled systems. The amplitude of thermal vibration are very low. This measurement provides the natural frequencies of the micro beam and their values depends on the actual geometry and dimension and the boundary conditions. To approximate the natural frequency of the micro beam in the linear regime and its corresponding mode shapes, theoretical calculation should be a good tool to use. Toward this, we refer back to Eq. 2.18 and set the forcing and damping terms equal to zero. In addition, to simplify the analysis, the axial force N is set equal to zero and EI is assumed constant. Therefore, the equation of motion is reduced to:

$$EI\frac{\partial^2 w}{\partial x^2} + \rho A\frac{\partial^2 w}{\partial t^2} = 0 \tag{3.1}$$

and the natural frequency is:

$$\omega_n = \sqrt{\frac{k}{m}} \tag{3.2}$$

where k is the effective stiffness and related to material characteristics, young's modulus and the moment of inertia.

$$k \propto EI \tag{3.3}$$

and inertia depends on the geometry of beam:

$$I = \frac{1}{12}bh^3 \tag{3.4}$$

therefore, the real factor of natural frequency approximation is:

$$\omega_n \propto \frac{Eh}{\rho l} \tag{3.5}$$

To measure the thermal natural frequency, we need to set four parameters for vibrometer controller. The first parameter is “range” which indicates the velocity factor of LDV. The second is the maximum frequency of analog decoders. The last two parameters define the frequency range of

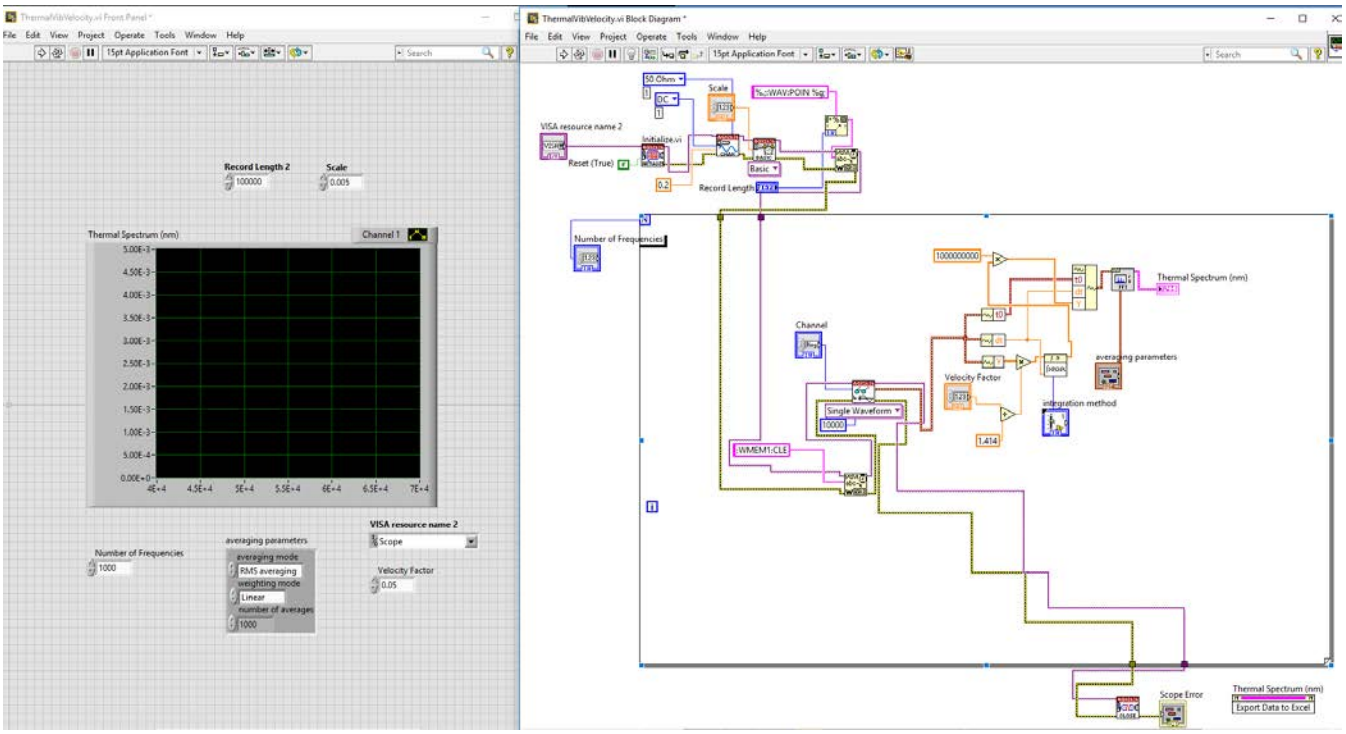

Figure 16: User interface panel and LabVIEW program diagram for the thermal frequency measurement

the filter. One LabVIEW program is used to control the function generator (input signal) and to collect the data from the oscilloscope (output signal). Figure 15 shows the LabVIEW interface and the control windows. The acquired data is used in MATLAB program to generate the plot of the thermal vibration. The plot evaluates the captured natural frequency of the beam.

The second step is to characterize the forced vibration of the beam. At this level, the micro beam is excited at its natural frequencies to exhibit natural mode shapes. The number of the captured natural frequencies by thermal frequency measurement, typically three, is limited by the limit of LDV capability (it goes only up to 20MHz). At each natural frequency, which corresponds to one natural

mode shape, the frequency response and the vibration amplitude measurement were performed at different locations in the beam using the new capability of the setup.

Here as we add the moving stage, a sub program has been added to the main LabVIEW program to manipulate the stage during measurement. Once everything is integrated, the new setup controlled with the new LabVIEW program makes possible the measurement of the dynamic response of the beam at different locations of the beam geometry. The measurement is continuous and stages are moving automatically for the next location (measurement point). The moving step is defined by giving the length of the beam and the number of points that will be covered. The custom LabVIEW will be introduced in Chapter 4.

Chapter 4: Results and Discussion

This Chapter covers two main parts: The first part describes the components and the steps to follow to build the control of the stages as an added value to the measurement procedure. In the second part the dynamic response measurement and mode shape are presented for two micro beams.

4.1 LabVIEW Programs

4.1.1 User Panel

Figure 16 shows the user panel of the main LabVIEW program. It includes the control of the stage, function generator control and data acquisition from the oscilloscope. From the user pannel one can check the status of the stage, set the parameters and read the measurements results.

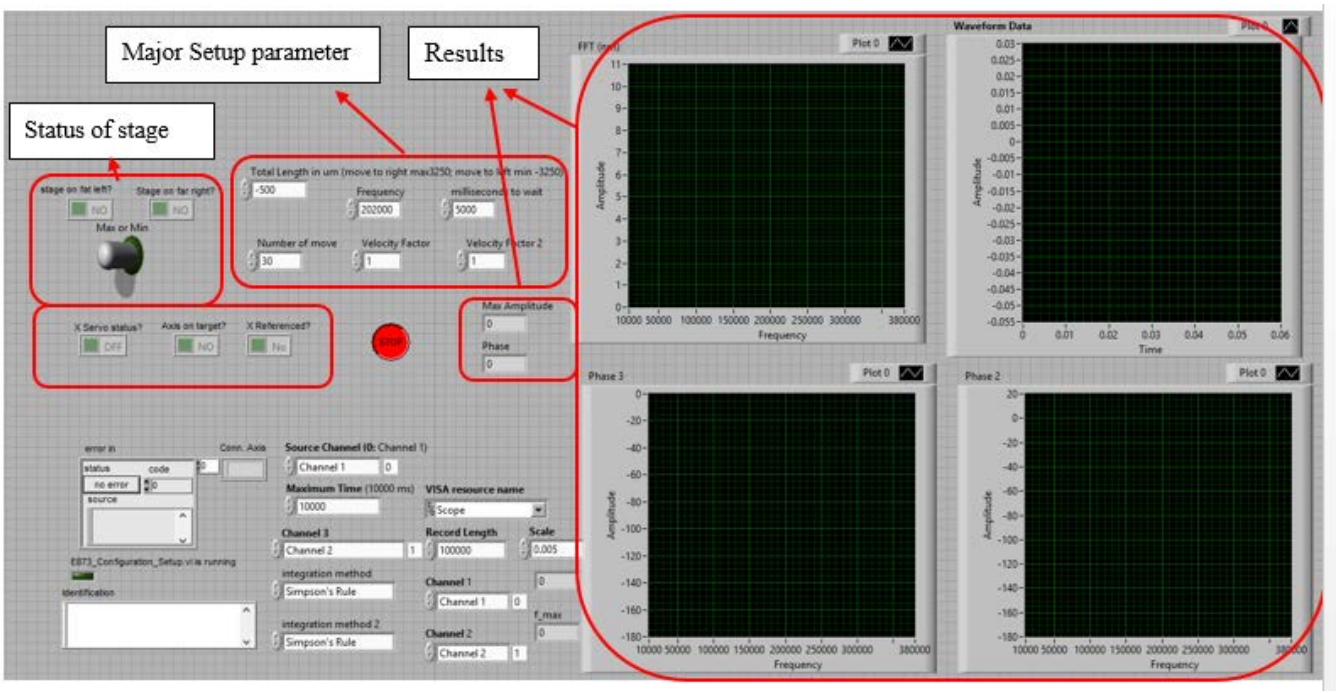

Figure 17: User Panel for the main LabVIEW program

Before running this program, four parameters need to be set. First we give the total length of the

microbeam in micrometer. The sign of value must be included because it indicates the orientation of moving stage. Positive sign indicates that the stage is moving to the right from starting point, and to the left at negative sign. The second parameter is the total scanning points N and it should be an integer. This value tells the stage how many movement needs to be achieved and it corresponds to N-1 steps. The step between two movements is calculated as the quotient of total length by total number of movement. The third parameter is the velocity factor which controls the vibrometer measurement. The last parameter is the frequency and it corresponds to one natural frequency of the beam. The value of the frequency indicates the mode frequency of the sample. This number is used to calculate two values of output, maximum amplitude value and phase value. The frequency response curve is also provided at each point measurement. When running the LabVIEW program, the delay time between moving the stage and measuring can be controlled.

4.1.2 Stage Controller Program

This section describes how to build custom LabVIEW program to control PI stage. This program is integrate in the main LabVIEW program (described earlier) to run the experiment.

The first step is running ‘E873_Configuration_Setup.vi’. This sub vi file will initialize vi with all necessary steps automatically. Then the following steps are performed in order: 1. Open the communications port. 2. Define the IDs for the connected axes. 3. Set references to the connected stages (if appropriate), depending on if the controller requires a referencing before axes can be moved and on your custom settings. 4. Define the controller name. After these steps, parameters are saved in global variables, so that other vis invoked during the same LabVIEW session can access this data at runtime. For successful run, we select the flowing setting shown in table 1. After running

‘E873_Configuration_Setup.vi’, this sub vi will communicate one cluster to the next sub vi which contain three elements, status, code and source. The other sub vis will do the same assignment and pass one cluster to the next sub vi function. Figure 17 shows the diagram of “E873_Configuration_Setup.vi” and its different components.

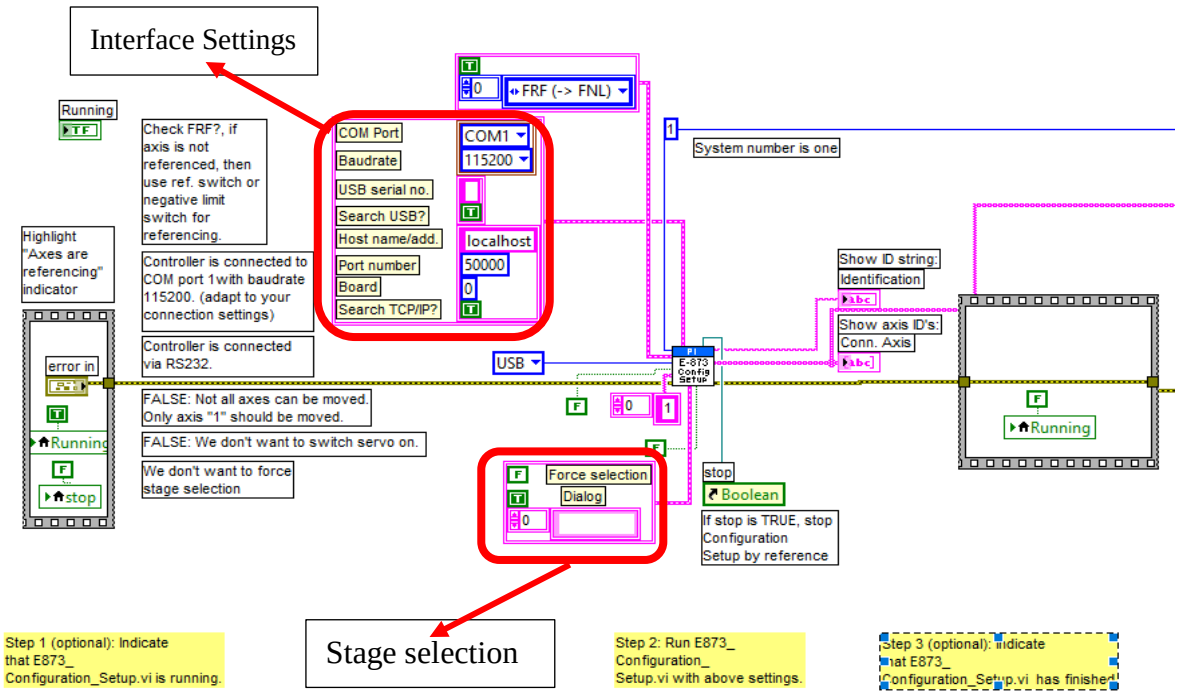

Figure 18: E873_Configuration_Setup.vi

Table 1 E873_Configuration_Setup value

Name of Input	Setting	Function
Interface Settings	Multiple value, shown in Fig,22	
System number	1	The 1 refers to the axis
Referencing	FRF	To reference the stage
Interface	USB	
All axes?	F	Only one axes
Axes to move	1	
Stage selection	Multiple value, shown in Fig,22	
Switch servo on?	F	Only check status of stage

The second step is to switch servo on. Utilized SVO and SVO? sub vis to achieve this goal. SVO can switch servo on and SVO? will check its status (if it is on and Return servo status of queried axes). The diagram of this sub vi is shown in figure 18. For successfully running SVO and SVO? , we select flowing settings, shown in table 2 and table 3.

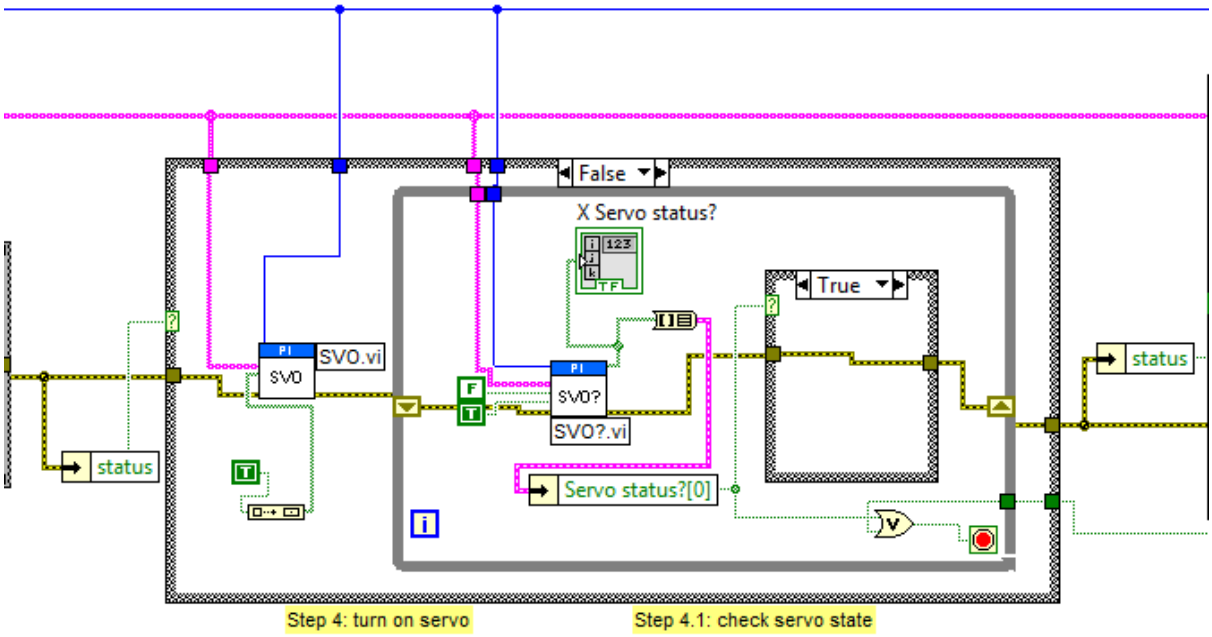

Figure 19: Switch Servo on program's diagram

Table 2 SVO settings

Name of input	Setting
System number	1
Without axis ID?	False
Axes to command	empty string array
Servo mode	empty array of false bool

Table 3 SVO? settings

Name of input	Setting
System number	1
Axes to query	empty string array
All axes?	False
Axis identifier?	Ture

Third step is to set a reference of the stage. Both FRF and FRF? sub vis are used to achieve this goal. FRF vi starts a fast referencing of the specified axes and FRF? will Indicates whether queried axes have been referenced, shown in figure 19. For successfully running FRF and FRF?, we select the appropriate settings, shown in table 4 and table 5. The program's diagram is shown in figure 19.

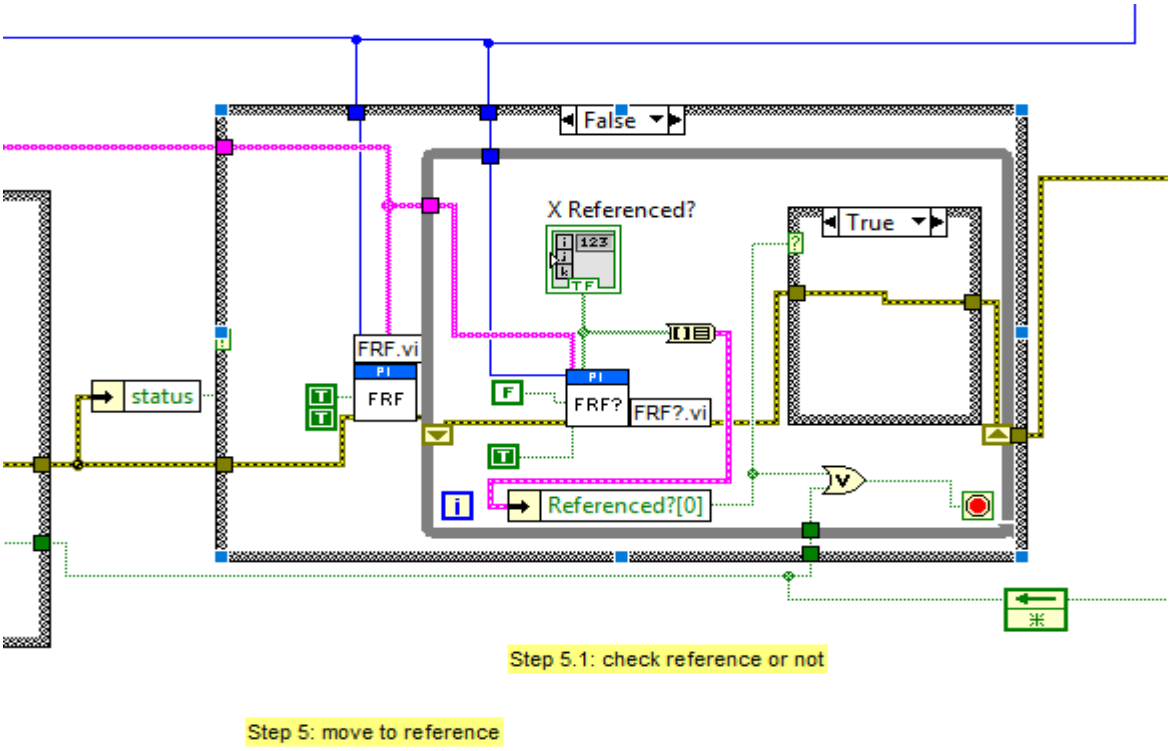

Figure 20: FRF and FRF? Program's diagram

Table 4 FRF settings

Name of input	Setting
System number	1
Affected axes	empty string array
All axes?	False
Axis identifier?	True

Table 5 FRF? settings

Name of input	Setting
System number	1
Affected axes	empty string array
All axes?	False
Axis identifier?	True

The fourth step is moving the stage to far left or far right position which is start point to measure. To do that we use MOV and ONT? sub vi. MOV vi Moves specified axes to specified absolute positions and ONT? will indicate whether queried axis is at target position or not, shown in figure 20. For successfully running MOV and ONT?, settings shown in table 6 and table 7 are selected. The program's diagram is shown in figure 20.

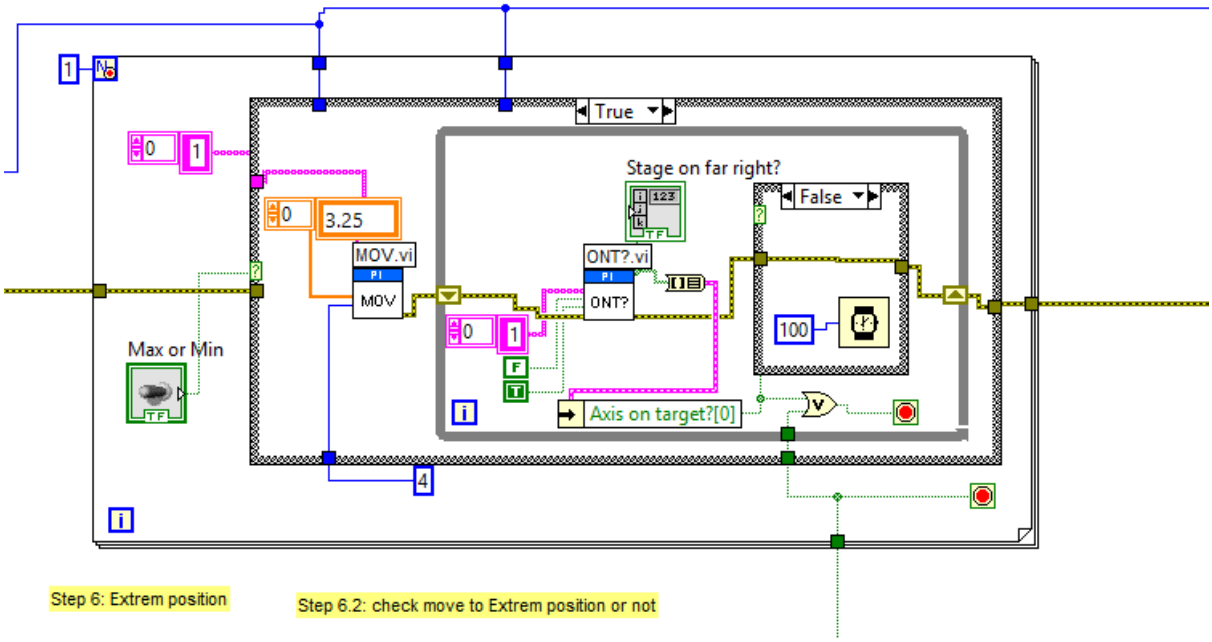

Figure 21: MOV and ONT? Program

Table 6 MOV settings

Name of input	Setting
System number	1
Axes to move	empty string array
Position values	3.25 or -3.25
No. of digits	4

Table 7 ONT? Settings

Name of input	Setting
System number	1
Axes to query	empty string array
All axes?	Fales
Axis identifier?	Ture

The fifth step is moving stage step by step. Both MVR and ONT? sub vis are called to achieve this goal. MOV vi moves specified axes relative to current position and ONT? check whether queried axis is at target position or not. Its diagram is shown in figure 21. Successful run of MOV vi is achieved under the settings shown in table 8. This section will return the final position of stage and record every movement and it is achieved by POS? function.

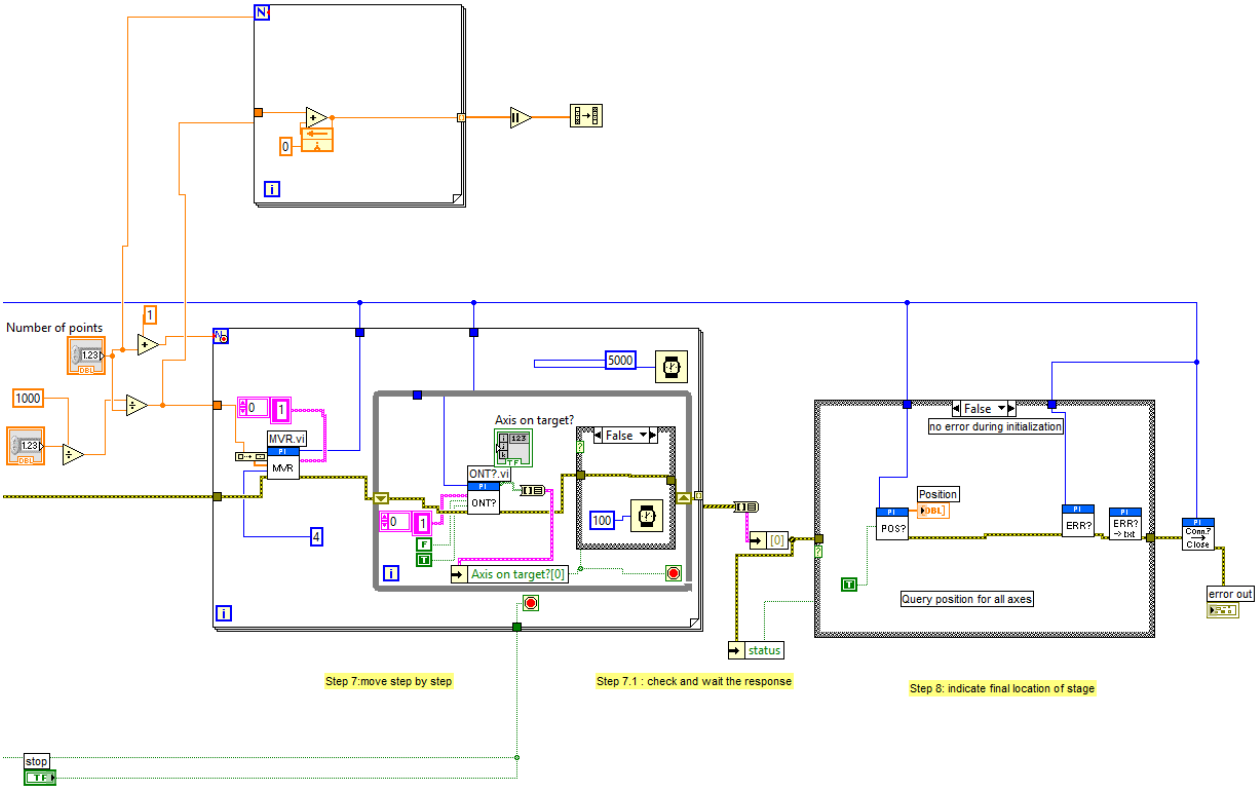

Figure 22: MVR and POS?

Table 8: MVR settings

Name of input	Setting
System number	1
Axes to query	Empty String Array
Position values	Resolution
No. of digits	4

The final step is to integrate all sub vi within the main measurement program. The overview of LabVIEW program shown in appendix.

4.2. Experimental results and processed data:

4.2.1 Micro cantilever beam

The first measurement is performed to identify the natural frequencies of the beam. Here the experimental characterization is performed for cantilever micro-beam. The dimensions of cantilever are L=500um, W=100um, t=2um as shown in the figure 15. Figure 22 shows the thermal frequency measurement for the cantilever structure and its natural frequencies. The natural frequency includes some bandwidth but the noise does not include. Therefore, table 9 shows the values of the three natural frequencies of the micro cantilever.

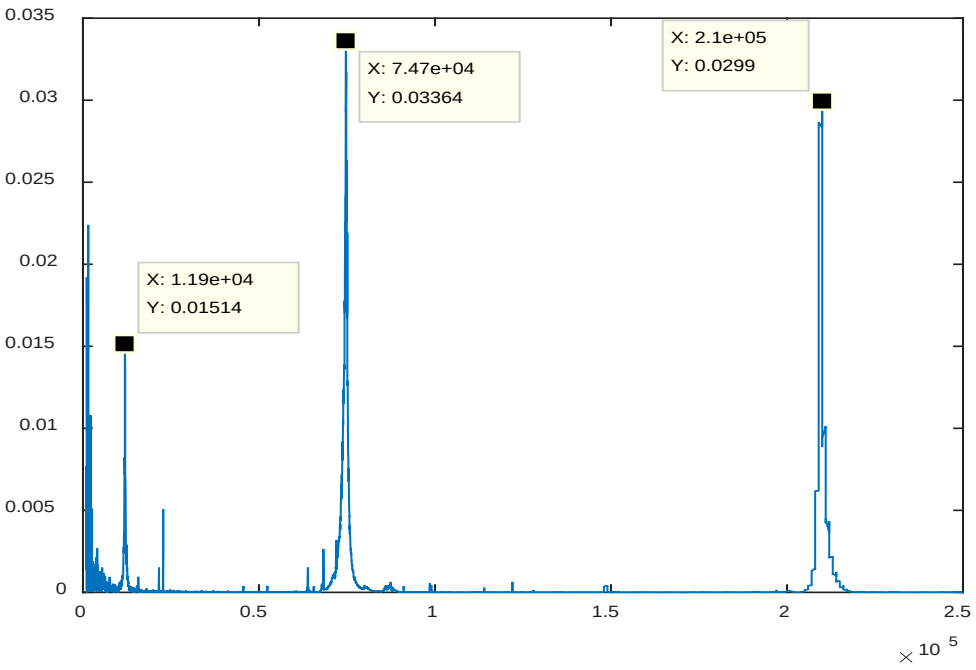

Figure 23: Thermal Frequency response showing the 3 first natural frequencies of silicon micro cantilever

Table 9 Natural frequencies of the micro cantilever beam

Mode shape	Frequency (kHz)
1	11.9
2	74.7
3	210

To capture the different mode shapes, the micro cantilever beam was excited at its natural frequencies and then the vibration amplitude is measured at different locations.

The figure 24 shows the frequency response under four different input voltage. All the response are linear.

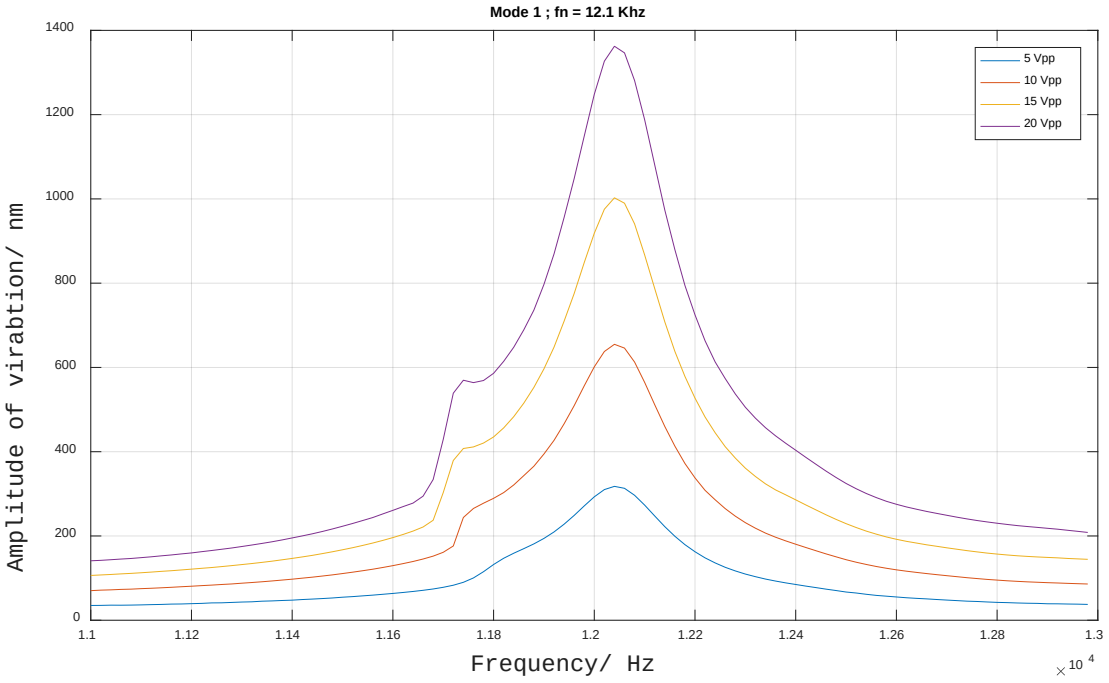

Figure 24: Frequency response of cantilever for first mode

The figures 25, 26, and 27 display the results of the 1st, 2nd and 3rd mode shape respectively for fixed-free micro beam sample. As the voltage increases, the amplitude of vibration is increasing. Each mode shape is identified by the number of the extremum in the vibration amplitude and the number of the stagnation points (zero amplitude). Those number are known to be 1, 2 and 3 extremums for the 1st, 2nd and 3rd mode shape respectively and 0, 1,2 stagnation points for the 1st, 2nd and 3rd mode shape respectively.

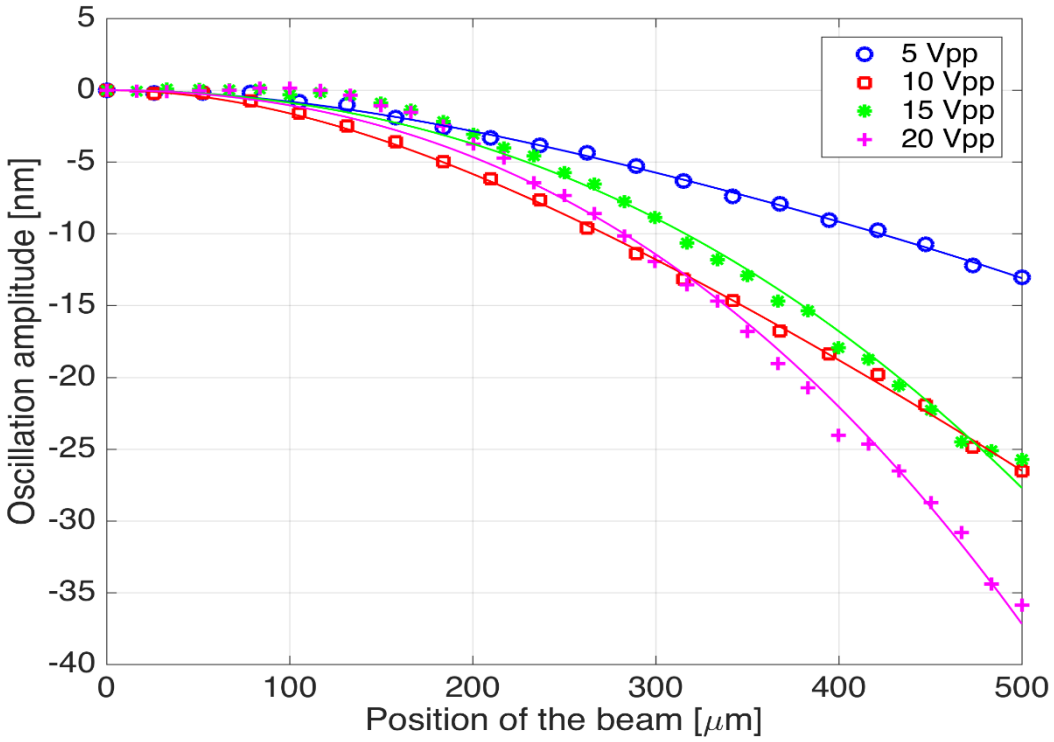

Figure 25: First mode shape of micro cantilever beam

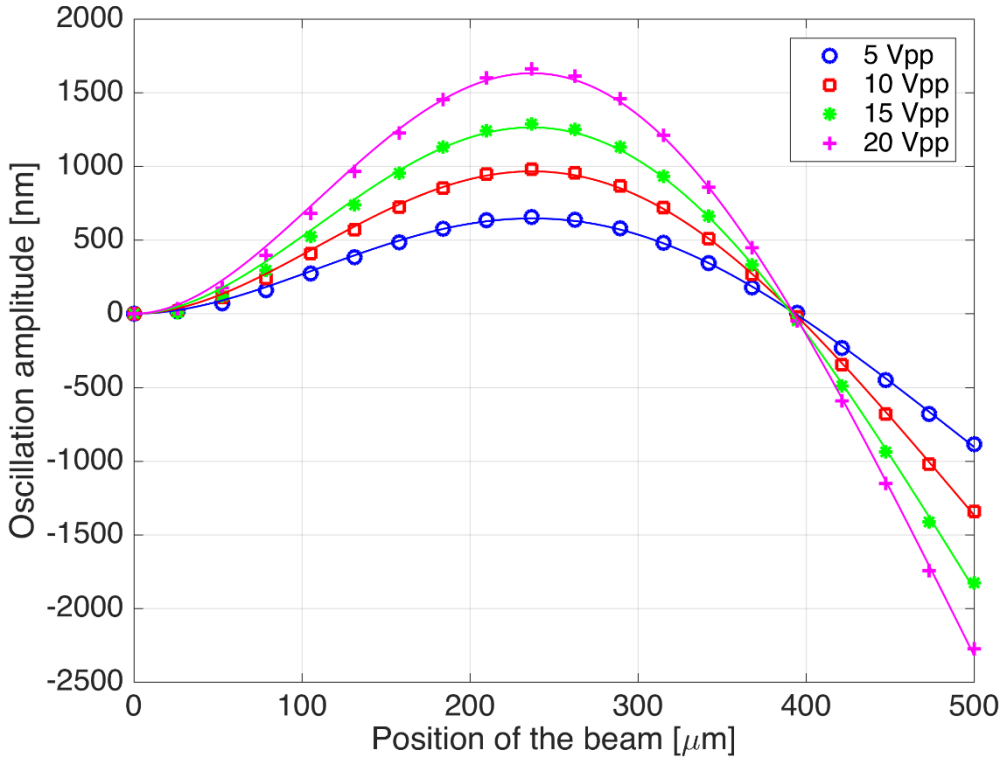

Figure 26: Second model shape of micro cantilever beam

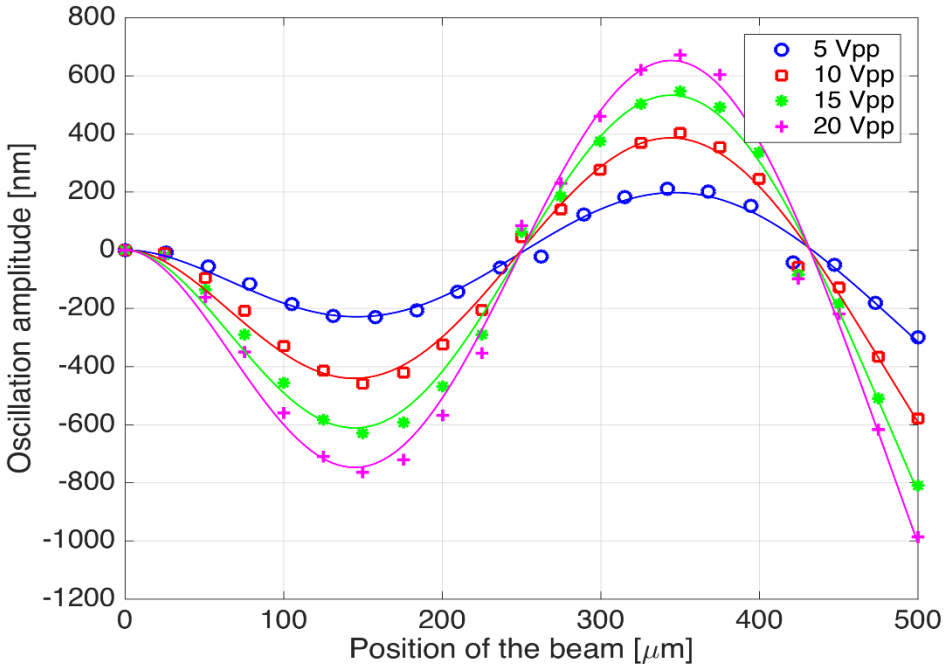

Figure 27: Third model shape of micro cantilever beam

For first mode, the maximum amplitude goes to 35 nm. For second mode, the maximum amplitude goes to 1660 nm on the top and 1774 nm underneath. For the third mode shape, the first peak shows at 157 um long from the fixed point and the maximum amplitude is 765 nm, the second peak shows at 367 um long from the fixed point and maximum amplitude is 672 nm.

From the theoretical side, the mode shape of a micro cantilever beam could be described by equation 2.22. The property of silicon material listed in table 10. Each value was used to get theoretical value of C, shown in table 11

Table 10 Silicon Material Properties

	Density	Young's Modulus	Width	Thickness	Length
Value	2330 kg/m^3	165 GPa	100 um	2 um	500um

Table 11 Theoretical coefficient value of c

	C1	C2	C3	C4
Mode 1 (11.9 KHz)	-1	0.734096	1	- 0.734096
Mode 2(74.7 KHz)	-1	1.018467	1	- 1.018467
Mode 3(210 KHz)	-1	0.999224	1	- 0.999224

Utilizing normalized function to generate normalized mode shape of experimental results and then compare to theoretical mode shape. Figure 26, 27 and 28 give the results.

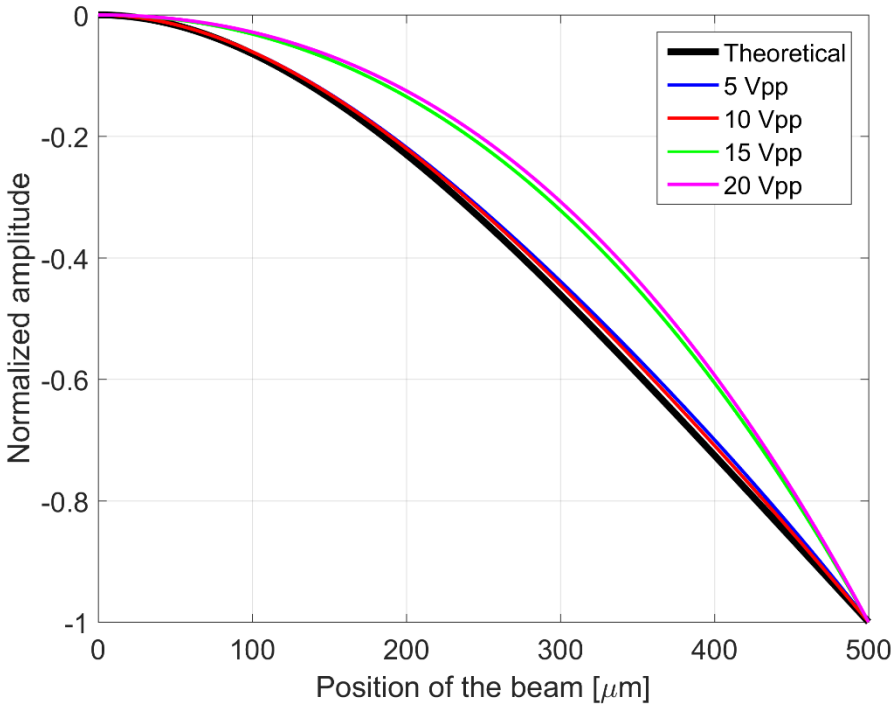

Figure 28 Normalized first mode shape of micro cantilever

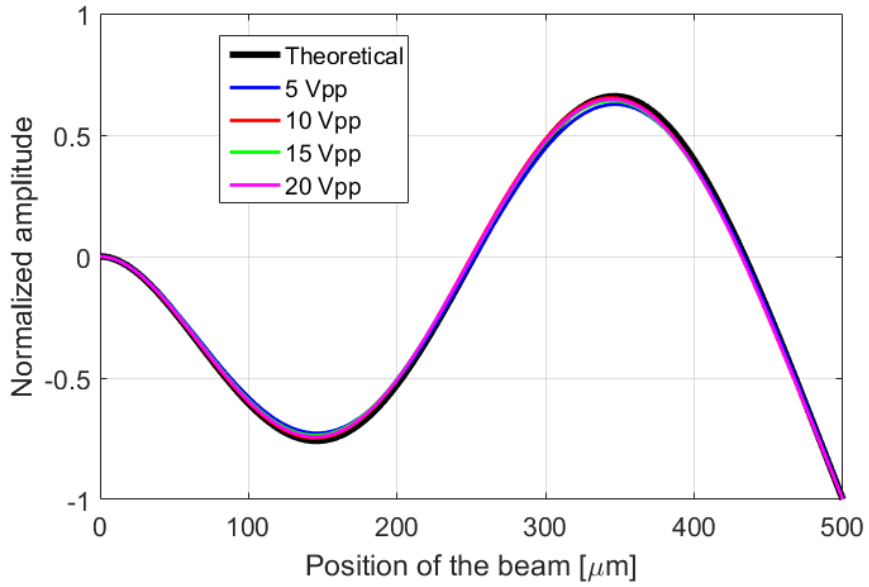

Figure 30 Normalized second mode shape of micro cantilever

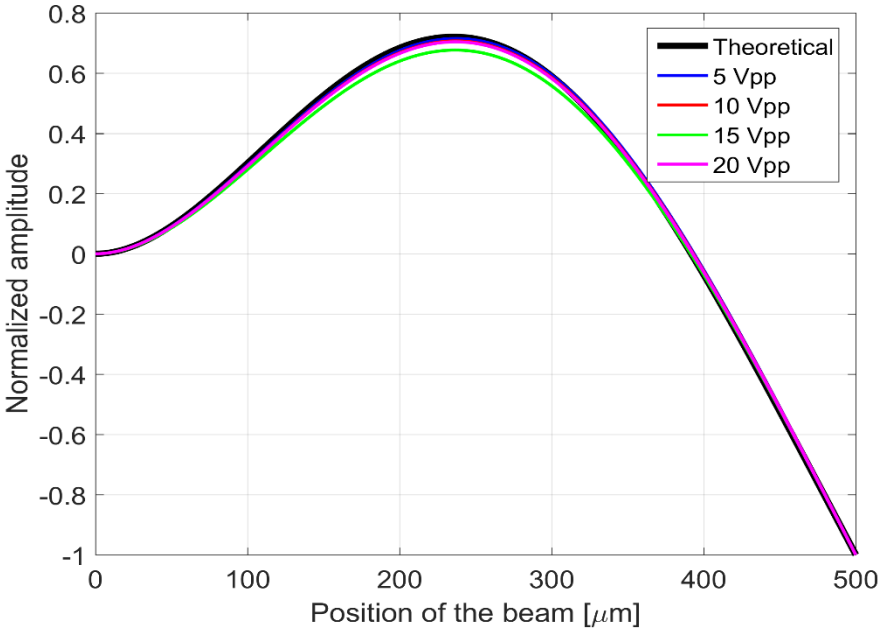

Figure 29: Normalized third mode shape of micro cantilever

For each normalized mode shape, they all have the same curve and same shape. The experimental normalized mode shapes are matched with theoretical mode shape. For the first mode shape of 15 V and 20 V conditions is little far away from theoretical mode shape. The reason can be nonlinearity has occurred. All other results are successful and acceptable.

4.2.2 Fixed-fixed micro beam:

The first measurement is performed to identify the natural frequencies of the beam. This is was done under thermal vibration for fixed-fixed polymer/silicon micro beam, its image is depicted in figure 29. The 3 first natural frequencies were detected from different pics in the vibration amplitude and they correspond to different mode shapes. Their values and their corresponding modes are shown in table 9. Figure 22 shows the thermal frequency measurement. The plot displays the vibration amplitude as a function of the frequency. Natural frequencies correspond to the frequencies (X axis values) of the different pics in the amplitude (Y axis).

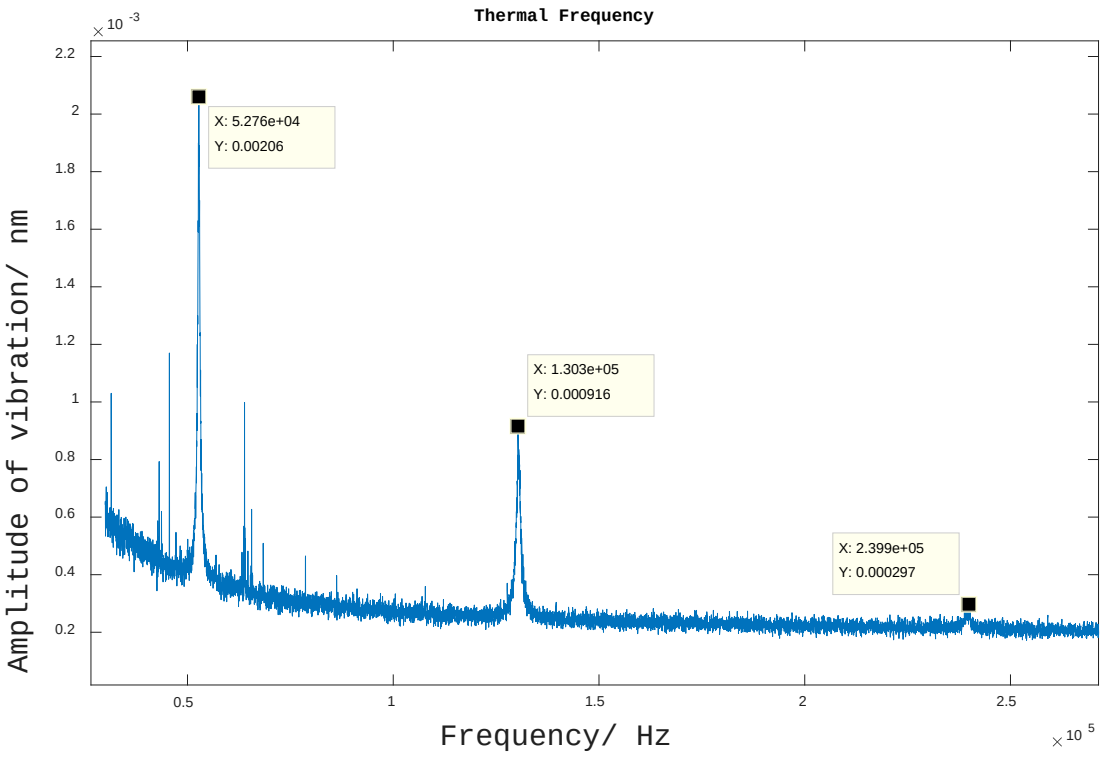

Figure 31 Thermal Frequency response showing the three first natural frequencies of polymer/silicon micro beam structure

Table 12 Natural frequencies of the fixed-fixed micro beam

Mode shape	Frequency (KHz)
1	52.8
2	130
3	239

Table 13 presents the measured results for 500um long beam at 31 different locations. The measurements are performed at the 3rd mode (233kHz) vibrating frequency and with 14V. The first measurement point is located near the edge of silicon beam/polymer attachment at a distance of 450 um from the anchored side of the silicon beam. Then the whole silicon beam have been scanned with 31 measurement points.

Table 13: measurement data

Location(mm)	Amplitude(nm)	Phase(degree)
0.450	5.596	157.478
0.435	2.259	146.577
0.421	1.817	-2.200
0.406	5.738	-8.776
0.392	9.320	-13.394
0.377	12.572	-12.576
0.363	14.455	-5.223
0.348	16.074	-12.260
0.334	16.312	-6.155
0.319	15.510	-18.420
0.305	13.843	-20.511
0.290	11.748	-13.314
0.276	8.881	-11.134
0.261	5.451	-14.541
0.247	1.665	11.109
0.232	2.536	144.752
0.218	6.052	154.565
0.203	9.013	162.354
0.189	12.042	161.661
0.174	14.727	161.029
0.160	15.909	164.780
0.145	16.790	169.746

0.131	17.069	163.774
0.116	16.437	164.740
0.102	14.855	173.716
0.087	12.709	165.292
0.073	10.530	165.077
0.058	7.766	162.938
0.044	5.168	166.067
0.029	2.627	155.626
0.015	0.626	151.967
0	0	0

Figure 30 shows the result of the measurement for fixed-fixed polymer/silicon beam sample at its first natural frequency (52.8 kHz). The same measurements have been repeated at different excitation voltages (5V, 10V, 14V, 18V, 20V). As the voltage increases, the amplitude of vibration was increased. The curve shows the mode shape of scanned silicon part of the beam only; it does not include the polymer part.

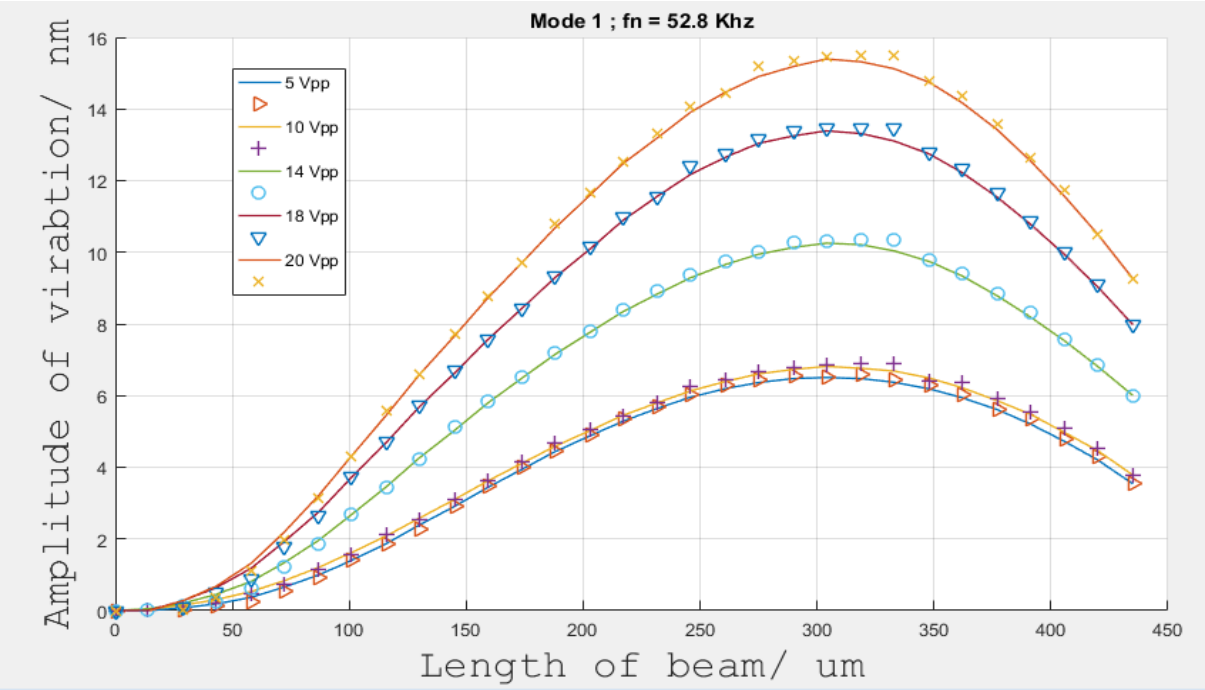

Figure 32: First mode shape of the fixed-fixed micro beam

All the amplitude curves show a unique pic (extremum, here is a maximum) which confirms the shape of the first mode. Also, no stagnation point (zero amplitude) is captured rather than the edge. The value of this pic depends on the excitation voltage. The same experimental steps have been performed to capture the 3rd mode shape of the micro beam.

Then an excitation frequency of 233 kHz is used with different voltage values (5V, 8V, 10V, 14V, 18V). Figure 31 plots the obtained mode shape. As it is mentioned previously, only the silicon part of the beam was scanned during the measurement, thus only 2 pics (one maximum and one minimum) are shown in the plot. However, two nodes points are detected: first point is located at 220um from the fixed edge and the second point is located at 420um from the fixed edge, which confirm the expected 3rd mode shape.

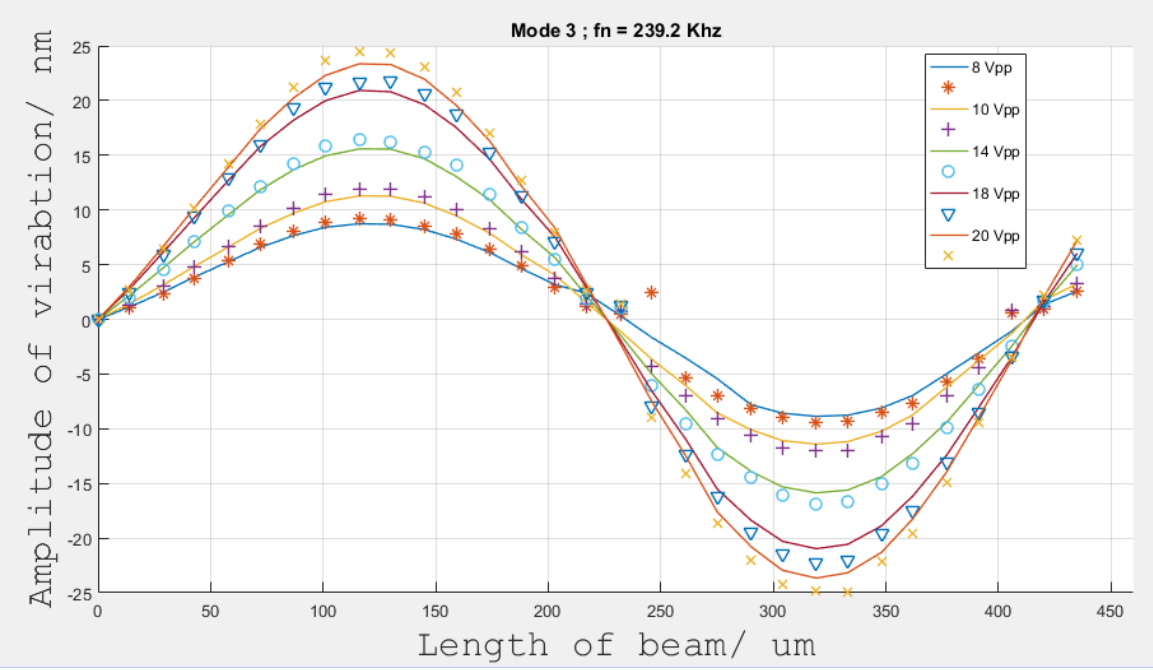

Figure 33: Third mode shape of the fixed-fixed micro beam

Further theoretical check was carried out to confirm the experimental investigation and state comparison between results. The mode shape of the fixed-fixed beam structure could be described

using the eigenvalue analysis to perform the dynamic analysis and determine the coefficients of mode shape equation 2.19.

We utilized “nlinfit” function in MATLAB to get the numerical expression of equation 2.19 and then compares to experimental results.

The calculated values of those coefficients for the 1st and 2nd mode shape are shown in table 14 and table 15 respectively.

Table 10 coefficient of first mode shape of fixed-fixed beam

	C1	C2	C3	C4
8Vpp	1	-6.4931	-0.9986	6.4759
10Vpp	1	-6.5684	-0.99885	6.5430
14Vpp	1	-7.0252	-0.99786	6.9600
18Vpp	1	-7.1758	-0.99763	7.0957
20Vpp	1	-7.2045	-0.99746	7.1197

Table 11 coefficient of second mode shape of fixed-fixed beam

	C1	C2	C3	C4
8Vpp	1	-4.5109	-1.0018	1
10Vpp	1	-4.5478	-1.0017	1
14Vpp	1	-4.5399	-1.0016	1
18Vpp	1	-4.5316	-1.0017	1
20Vpp	1	-4.5360	-1.0017	1

where C1, C2, C3, and C4 are the coefficient ratio by following equation:

$$C_I = \frac{c_i}{c1}; i = 1, 2,3,4 \tag{3.1}$$

Since the measurements are performed only on the silicon part, the fitting results doesn’t correspond to the accurate mode shape function. However once normalized within the same frame their comparisons make sense.

Chapter 5: Conclusion and Future Works

This research presents an experimental identification of mode shapes for vibrating micro beam. However, a theoretical study of the linear and nonlinear vibration regimes has been covered as well. As a start point, an old experimental setup has been and this allows only single point measurement which was not enough to build the mode shape of the structure. Then most part of this research was allocated to build an automatic measurement setup that covers different locations in the structure geometry. The requirement was to custom a general and flexible LabVIEW control program. The design of the setup takes in consideration the limitations and the sensitivity of the stage and a minimum step size of 4nm is allowable which is very accurate for micro scale structures.

As accuracy is concerned, as we increase the number of the scanned point as clear and more defined the mode shape is. Also here only the scan in the X axis is presented which draws only 1D (line) mode shape, however combining the measurements in two axes (X and Y) will provide a 2D (surface) images of the mode shape.

Giving the size of the moving stage, the actual measurements were conducted in ambient air condition which increase the error factor and add unwanted factors specially the air damping. Thus a further work will be carried out to perform the experiment in large vacuum chamber in order to exclude external factors. Different results is expected to be generated and would be more accurate

References

[1] Y. Développement, "MEMS Markets Status of the MEMS Industry 2015.," 2015.

[2] Z. S. a. I. Stanimirović, "Mechanical Properties of MEMS Materials," December 1, 2009.

[3] "MEMS Sensors for automotive appkications, life.augmented," [Online]. Available: http://www.st.com/en/mems-and-sensors.html.

[4] "MEMS in Healthcare," [Online]. Available: http://www.eeherald.com/section/design-guide/mems_medical.html.

[5] H. X. T. &. M. L. R. Mo Li1, "Ultra-sensitive NEMS-based cantilevers for sensing, scanned probe and very high-frequency applications," *Nature Nanotechnology,* 2007.

[6] "Introduction to Microelectromechanical Systems (MEMS)," [Online]. Available: https://compliantmechanisms.byu.edu/content/introduction-microelectromechanical-systems-mems.

[7] T. I. T. R. f. Semiconductors, "Micro-Electro-Mechanical Systems (MEMS)," 2013.

[8] R. L. a. M. C. Cross, "Nonlinear Dynamics of Nanomechanical and Micromechanical Resonators".

[9] L. G. Villanueva, "Nonlinearity in nanomechanical cantilever," 2013.

[10] LabVIEW (Vison 2015).

Appendix:

Custom LabVIEW part 1

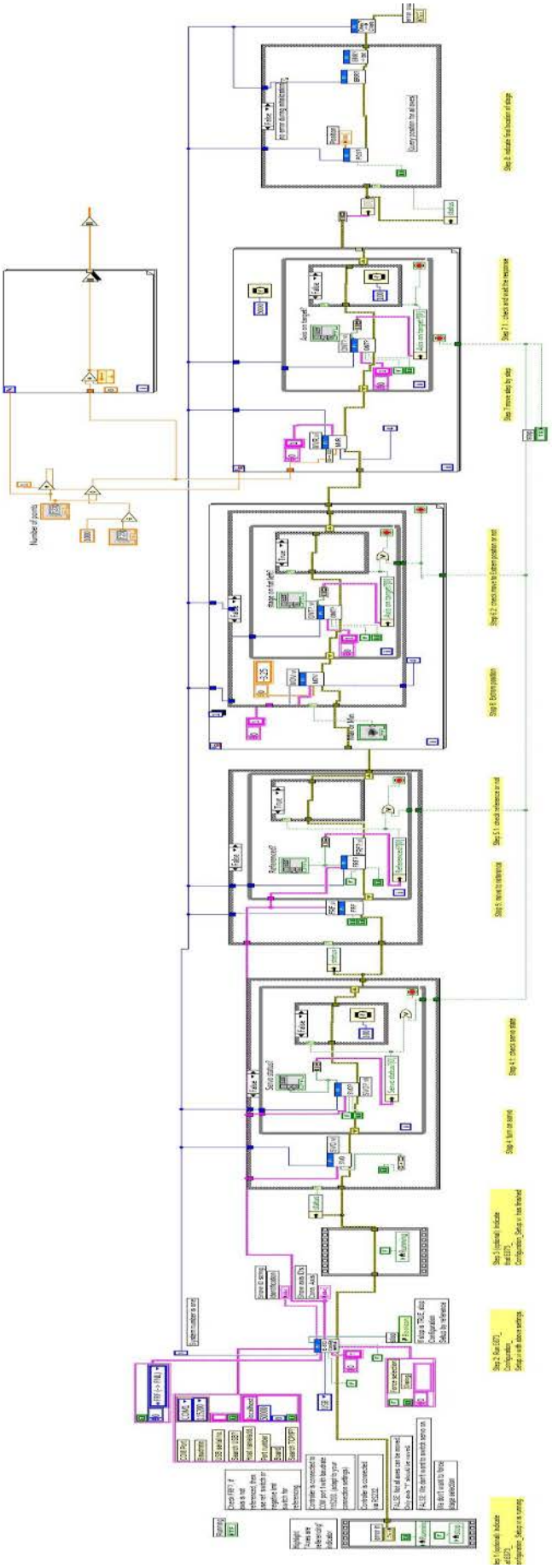

Custom LabVIEW part 2

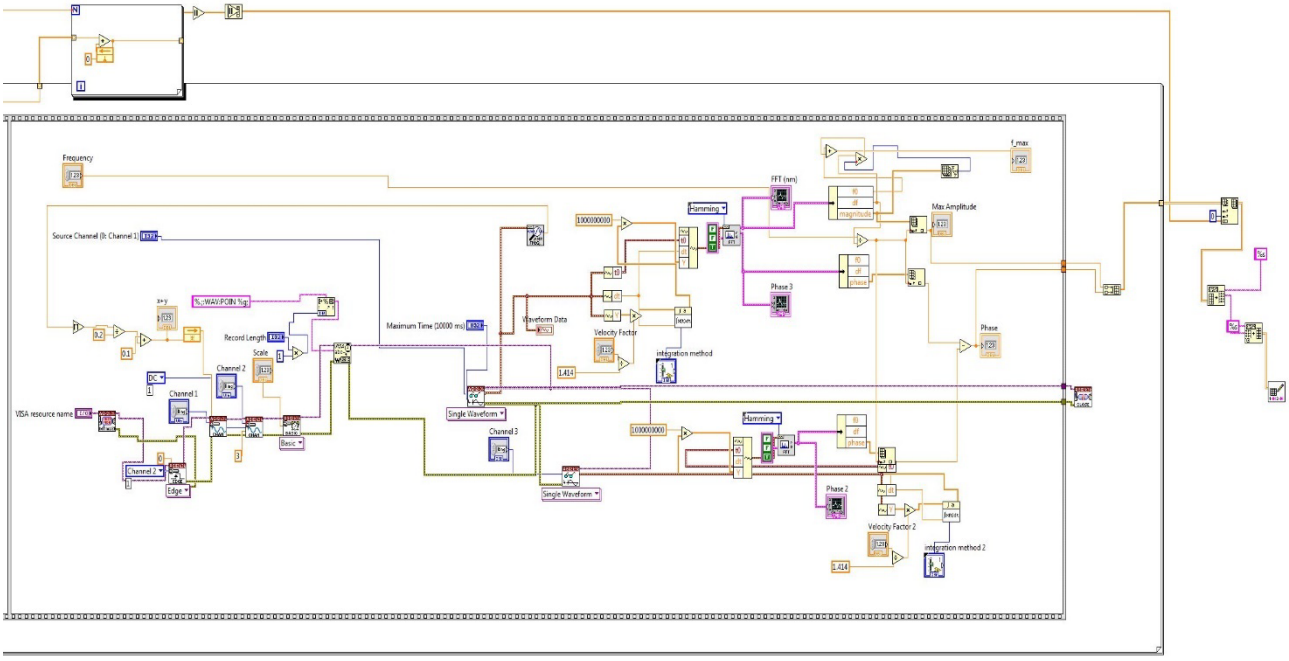

MATLAB code

for free-fixed beam

```
clc;clear all; close all;

load V5test1.txt
load V10test1.txt
load V15test1.txt
load V20test1.txt

L=0.5; %[mm]

%% 5V
L5 = V5test1(:,1);
A5 = V5test1(:,2);
P5 = V5test1(:,3);
n5 = length(P5);

for i = 1:n5
    if P5(i)<=0
        A5(i)=-A5(i);
    end
    if P5(i)>0
        A5(i)=A5(i);
    end
end

A5 = (A5-A5(1));
L5 = (L5-L5(1))/(L5(n5)-L5(1))*L;

c50 = [max(abs(A5))/2 9.388 1];

modelfun5 = @(c5,x)c5(1)*(-cos(c5(2)*x)+c5(3)*sin(c5(2)*x)+1*cosh(c5(2)*x)-
c5(3)*sinh(c5(2)*x));
c5f = nlinfit(L5,A5,modelfun5,c50);

%% 10V

L10 = V10test1(:,1);
A10 = V10test1(:,2);
P10 = V10test1(:,3);
n10 = length(P10);
```

```
for i = 1:n10
    if P10(i)<=0
        A10(i)=-A10(i);
    end
    if P10(i)>0
        A10(i)=A10(i);
    end
end

A10 = (A10-A10(1));
L10 = (L10-L10(1))/(L10(n10)-L10(1))*L;

c100 = [max(abs(A10))/2 9.388 1];

modelfun10 = @(c10,x)c10(1)*(-
cos(c10(2)*x)+c10(3)*sin(c10(2)*x)+1*cosh(c10(2)*x)-c10(3)*sinh(c10(2)*x));
c10f = nlinfit(L10,A10,modelfun10,c100);


%% 15
L15 = V15test1(:,1);
A15 = V15test1(:,2);
P15 = V15test1(:,3);
n15 = length(P15);

for i = 1:n15
    if P15(i)<=0
        A15(i)=-A15(i);
    end
    if P15(i)>0
        A15(i)=A15(i);
    end
end

A15 = (A15-A15(1));
L15 = (L15-L15(1))/(L15(n15)-L15(1))*L;

c150 = [max(abs(A15))/2 9.388 1];

modelfun15 = @(c15,x)c15(1)*(-
cos(c15(2)*x)+c15(3)*sin(c15(2)*x)+1*cosh(c15(2)*x)-c15(3)*sinh(c15(2)*x));
```

```
c15f = nlinfit(L15,A15,modelfun15,c150);
%%
L20 = V20test1(:,1);
A20 = V20test1(:,2);
P20 = V20test1(:,3);
n20 = length(P20);
for i = 1:n20

    if P20(i)<=0
        A20(i)=-A20(i);
    end

    if P20(i)>0
        A20(i)=A20(i);
    end

end

A20 = (A20-A20(1));
L20 = (L20-L20(1))/(L20(n20)-L20(1))*L;

c200 = [max(abs(A20))/2 9.388 1];

modelfun20 = @(c20,x)c20(1)*(-
cos(c20(2)*x)+c20(3)*sin(c20(2)*x)+1*cosh(c20(2)*x)-c20(3)*sinh(c20(2)*x));
c20f = nlinfit(L20,A20,modelfun20,c200)

%% figure(1)

figure(1)

% experimental data
plot(L5*1000,A5,'bo','LineWidth',2, 'MarkerSize',7); hold on
plot(L10*1000,A10,'rs','LineWidth',2, 'MarkerSize',7)
plot(L15*1000,A15,'g*','LineWidth',2, 'MarkerSize',7)
plot(L20*1000,A20,'m+','LineWidth',2, 'MarkerSize',7)

% calculate fittings
xx=linspace(0,0.5,1000);
ww5=c5f(1)*(-cos(c5f(2)*xx)+c5f(3)*sin(c5f(2)*xx)+1*cosh(c5f(2)*xx)-
c5f(3)*sinh(c5f(2)*xx));
ww10=c10f(1)*(-cos(c10f(2)*xx)+c10f(3)*sin(c10f(2)*xx)+1*cosh(c10f(2)*xx)-
```

```
c10f(3)*sinh(c10f(2)*xx));
ww15=c15f(1)*(-cos(c15f(2)*xx)+c15f(3)*sin(c15f(2)*xx)+1*cosh(c15f(2)*xx)-
c15f(3)*sinh(c15f(2)*xx));
ww20=c20f(1)*(-cos(c20f(2)*xx)+c20f(3)*sin(c20f(2)*xx)+1*cosh(c20f(2)*xx)-
c20f(3)*sinh(c20f(2)*xx));

% plot fittings
plot(xx*1000,ww5,'b','Linewidth',1)
plot(xx*1000,ww10,'r','Linewidth',1)
plot(xx*1000,ww15,'g','Linewidth',1)
plot(xx*1000,ww20,'m','Linewidth',1); hold off

xlabel ('Position of the beam [\mum]','FontSize', 18)
ylabel ('Oscillation amplitude [nm]','FontSize', 18)
legend('5 Vpp','10 Vpp','15 Vpp','20 Vpp')
set(gca,'Fontsize',16)
grid on

print('cant_mode1_a','-dtiff','-r300')

%%
% theoretical value of c
L=500e-6;
Ct1 = -1 ;
Ct3 = 1;
betaL=1.875;
beta=betaL/L;
Ct2 = (cosh(betaL)+cos(betaL))/(sinh(betaL)+sin(betaL));
Ct4 = -Ct2;

x = (0:1e-6:L);
fprintf('theoretical  value of C1 is %f, C2 is %f, C3 is %f, C4
is %f\n',Ct1,Ct2,Ct3,Ct4)
w = Ct1*cos(beta*x)+Ct2*sin(beta*x)+Ct3*cosh(beta*x)+Ct4*sinh(beta*x);

%normalize
w=w/max(abs(w));

ww5=ww5/max(abs(ww5));
ww10=ww10/max(abs(ww10));
ww15=ww15/max(abs(ww15));
ww20=ww20/max(abs(ww20));
```

```
figure(2)
plot(x*1e6,-w,'k','LineWidth',4, 'MarkerSize',7)
hold on
plot(xx*1e3,ww5,'b','LineWidth',2, 'MarkerSize',7)
plot(xx*1e3,ww10,'r','LineWidth',2, 'MarkerSize',7)
plot(xx*1e3,ww15,'g','LineWidth',2, 'MarkerSize',7)
plot(xx*1e3,ww20,'m','LineWidth',2, 'MarkerSize',7)

hold off

%title('Mode 1 ; f_n = 11.9 kHz')
xlabel ('Position of the beam [\mum]','FontSize', 18)
ylabel ('Normalized amplitude','FontSize', 18)
set(gca,'Fontsize',16)
legend('Theoretical','5 Vpp','10 Vpp','15 Vpp','20 Vpp')
grid on
print('cant_mode1_b','-dtiff','-r300')

 Fixed-Fixed beam
clc;clear all; close all;
format short
load V5test1.txt
load V8test1.txt
load V10test1.txt
load V14test1.txt
load V18test1.txt
load V20test1.txt


% 5Vpp conditions

L5 = V5test1(:,1);
A5 = V5test1(:,2);
P5 = V5test1(:,3);
n5 = length(P5);
for i = 1:n5

    if P5(i)<=0
        A5(i)=-A5(i);
    end
```

```
    if P5(i)>0
        A5(i)=A5(i);
    end

end
A5 = A5-A5(31);
L5 = L5-L5(31);

c50 = [1 1 1 1];
modelfun5 = @(c5,x)(c5(1)*cos(x)+c5(2)*sin(x)+c5(3)*cosh(x)+c5(4)*sinh(x));
beta5 = nlinfit(L5,A5,modelfun5,c50);
fprintf('The model function
is: %f*cos(x)+%f*sin(x)+%f*cosh(x)+%f*sinh(x)\n',beta5(1),beta5(2),beta5(3),beta5
(4))
C5 = beta5./beta5(1);
% 8Vpp conditions



% 10Vpp conditions

L10 = V10test1(:,1);
A10 = V10test1(:,2);
P10 = V10test1(:,3);
n10 = length(P10);
for i = 1:n10

    if P10(i)<=0
        A10(i)=-A10(i);
    end

    if P10(i)>0
        A10(i)=A10(i);
    end

end
A10 = A10-A10(31);
L10 = L10-L10(31);
c100 = [1 1 1 1];
modelfun10 = @(c10,x)(c10(1)*cos(x)+c10(2)*sin(x)+c10(3)*cosh(x)+c10(4)*sinh(x));
beta10 = nlinfit(L10,A10,modelfun10,c100);
fprintf('The model function
```

```
is: %f*cos(x)+%f*sin(x)+%f*cosh(x)+%f*sinh(x)\n',beta10(1),beta10(2),beta10(3),be
ta10(4))
C10 = beta10./beta10(1);

% 14Vpp conditions

L14 = V14test1(:,1);
A14 = V14test1(:,2);
P14 = V14test1(:,3);
n14 = length(P14);
for i = 1:n14

    if P14(i)<=0
        A14(i)=-A14(i);
    end

    if P14(i)>0
        A14(i)=A14(i);
    end

end
A14 = A14-A14(31);
L14 = L14-L14(31);
c140 = [1 1 1 1];
modelfun14 = @(c14,x)(c14(1)*cos(x)+c14(2)*sin(x)+c14(3)*cosh(x)+c14(4)*sinh(x));
beta14 = nlinfit(L14,A14,modelfun14,c140);
fprintf('The model function
is: %f*cos(x)+%f*sin(x)+%f*cosh(x)+%f*sinh(x)\n',beta14(1),beta14(2),beta14(3),be
ta14(4))
C14 = beta14./beta14(1);
% 18Vpp conditions

L18 = V18test1(:,1);
A18 = V18test1(:,2);
P18 = V18test1(:,3);
n18 = length(P18);
for i = 1:n18

    if P18(i)<=0
        A18(i)=-A18(i);
    end
```

```
    if P18(i)>0
        A18(i)=A18(i);
    end

end
A18 = A18-A18(31);
L18 = L18-L18(31);
c180 = [1 1 1 1];
modelfun18 = @(c18,x)(c18(1)*cos(x)+c18(2)*sin(x)+c18(3)*cosh(x)+c18(4)*sinh(x));
beta18 = nlinfit(L18,A18,modelfun18,c180);
fprintf('The model function
is: %f*cos(x)+%f*sin(x)+%f*cosh(x)+%f*sinh(x)\n',beta18(1),beta18(2),beta18(3),be
ta18(4))
C18 = beta18./beta18(1);

% 20Vpp conditions

L20 = V20test1(:,1);
A20 = V20test1(:,2);
P20 = V20test1(:,3);
n20 = length(P20);
for i = 1:n20

    if P20(i)<=0
        A20(i)=-A20(i);
    end

    if P20(i)>0
        A20(i)=A20(i);
    end

end
 A20 = A20-A20(31);
 L20 = L20-L20(31);
c200 = [1 1 1 1];
modelfun20 = @(c20,x)(c20(1)*cos(x)+c20(2)*sin(x)+c20(3)*cosh(x)+c20(4)*sinh(x));
beta20 = nlinfit(L20,A20,modelfun20,c200);
fprintf('The model function
is: %f*cos(x)+%f*sin(x)+%f*cosh(x)+%f*sinh(x)\n',beta20(1),beta20(2),beta20(3),be
ta20(4))
C20 = beta20./beta20(1);
```

```
c1 = [C5(1);C10(1);C14(1);C18(1);C20(1)];
c2 = [C5(2);C10(2);C14(2);C18(2);C20(2)];
c3 = [C5(3);C10(3);C14(3);C18(3);C20(3)];
c4 = [C5(4);C10(4);C14(4);C18(4);C20(4)];
Name = {'5Vpp','10Vpp','14Vpp','18Vpp','20Vpp'};
T = table(c1,c2,c3,c4,'RowNames',Name)

%  A moving average filter smooths data
%  by replacing each data point with the average of the neighboring
%  data points defined within the span
hold on
grid on
A55 = smooth(A5);
plot (L5*1000,A55,L5*1000,A5,'>','LineWidth',1, 'MarkerSize',7)

A100 = smooth(A10);
plot (L10*1000,A100,L10*1000,A10,'+','LineWidth',1, 'MarkerSize',7)

A1414 = smooth(A14);
plot (L14*1000,A1414,L14*1000,A14,'o','LineWidth',1, 'MarkerSize',7)

A1818 = smooth(A18);
plot (L18*1000,A1818,L18*1000,A18,'v','LineWidth',1, 'MarkerSize',7)

A2020 = smooth(A20);
plot (L20*1000,A2020,L20*1000,A20,'x','LineWidth',1, 'MarkerSize',7)

title('Mode 3 ; fn = 239.2 Khz')
xlabel ('Length of beam/ um','FontSize', 22, 'FontName', 'FixedWidth')
ylabel ('Amplitude of virabtion/ nm','FontSize', 22, 'FontName', 'FixedWidth')
legend('5 Vpp','','10 Vpp','','14 Vpp','','18 Vpp','','20 Vpp','')
xlim([0 450])
ylim([0 16])

figure;
hold on
grid on
A5m = max(abs(A5));
A5n = A5/(A5m);
A55n = smooth(A5n);
```

```
plot(L5*1000,A55n)

A10m = max(abs(A10));
A10n = A10/(A10m);
A1010n = smooth(A10n);
plot(L10*1000,A1010n)

A14m = max(abs(A14));
A14n = A14/(A14m);
A1414n = smooth(A14n);
plot(L14*1000,A1414n)

A18m = max(abs(A18));
A18n = A18/(A18m);
A1818n = smooth(A18n);
plot(L18*1000,A1818n)

A20m = max(abs(A20));
A20n = A20/(A20m);
A2020n = smooth(A20n);
plot(L20*1000,A2020n)
title('Mode 3 ; fn = 239.2 Khz')
xlabel ('Length of beam/ um','FontSize', 18, 'FontName', 'FixedWidth')
ylabel ('Amplitude of virabtion/ nm','FontSize', 18, 'FontName', 'FixedWidth')
legend('5 Vpp','10 Vpp','14 Vpp','18 Vpp','20 Vpp')
```